

**UNIVERSIDADE DO VALE DO RIO DOS SINOS - UNISINOS
UNIDADE ACADÊMICA DE PESQUISA E PÓS-GRADUAÇÃO
PROGRAMA DE PÓS-GRADUAÇÃO EM GEOLOGIA
NÍVEL MESTRADO**

**DEFESA DE MESTRADO
EDUARDO GUARESCHI MÜLLER**

**GÊNESE DE CONCENTRAÇÕES DENSAMENTE FOSSILÍFERAS DO
EOCENO MÉDIO, FORMAÇÃO MAN AIKE, BACIA FORELAND
MAGALLANES (PATAGÔNIA CHILENA)**

São Leopoldo

2021

EDUARDO GUARESCHI MÜLLER

**GÊNESE DE CONCENTRAÇÕES DENSAMENTE FOSSILÍFERAS DO
EOCENO MÉDIO, FORMAÇÃO MAN AIKE, BACIA FORELAND
MAGALLANES (PATAGÔNIA CHILENA)**

Área de Concentração: Geologia Sedimentar

Linha de Pesquisa: Paleontologia Aplicada

Tema de interesse: Tafonomia– Geoquímica

Dissertação de mestrado apresentada como requisito parcial para obtenção do título de Mestre em Geologia, pelo Programa de Pós-Graduação em Geologia da Universidade do Vale do Rio dos Sinos (UNISINOS).

Orientador: Prof. Dr. Rodrigo Scalise Horodyski

Coorientador: Prof. Dr. Karlos G. D. Kochhann

M958g

Müller, Eduardo Guareschi.

Gênese de concentrações densamente fossilíferas do Eoceno médio, formação man aiike, bacia foreland Magallanes (Patagônia Chilena). / Eduardo Guareschi Müller. – 2021.

69 f. : il. ; 30 cm.

Dissertação (mestrado) – Universidade do Vale do Rio dos Sinos, Programa de Pós-Graduação em Geologia, 2021.

“Orientador: Prof. Dr. Rodrigo Scalise Horodyski

Coorientador: Prof. Dr. Karlos G. D. Kochhann”

1. Bacia de Magallanes. 2. Depósito marinho. 3. Eoceno médio. 4. Fossilíferas. I. Título.

CDU 55

Dados Internacionais de Catalogação na Publicação (CIP)
(Bibliotecária: Silvana Dornelles Studzinski – CRB 10/2524)

RESUMO

Nos depósitos marinhos do Eoceno-médio da região de Magallanes, Província de Última Esperanza (Chile), encontram-se concentrações fossilíferas associadas a depósitos siliciclásticos marinho raso. Durante este período, oscilações climáticas e mudanças globais de circulação marinha ocorreram registrando variações do nível relativo do mar na região sul da Placa Sul Americana e na Antártica. Na borda noroeste da Bacia de Magallanes, na localidade de El Puesto (Vale do Rio de Las Chinas, Patagonia Chilena), afloram depósitos de granulometria grossa, siliciclástica, intercalados com concentrações fossilíferas densas representando parte da deposição do Eoceno-médio. Buscando aprimorar interpretações paleoambientais, o presente estudo apresenta uma caracterização *multi-proxy*, baseada em análises de fácies, tafonomia e análise de FRX (Fluorescência de Raio-X), a fim de entender a gênese das concentrações densamente fossilíferas da Formação Man Aike. A base da Formação Man Aike apresenta como depósitos transgressivos de *shoreface*. Os resultados corroboram com as interpretações prévias de uma deposição em ambiente marinho raso de *shoreface* superior transicionando para *shoreface* inferior, sob influência de processos de alta energia com deposição controlada por correntes e ondas. As concentrações fossilíferas indicam uma deposição sob a ação de ondas de tempo bom e ondas de tempestades, relacionados a tempestitos proximais e distais. Os depósitos proximais são interpretados como *lag concentrations*. Outro registro diz respeito a depósitos hiatais com formação de *event concentrations* (associações fossilíferas do tipo senso ecológico) e depósitos episódicos relacionados a debris flows. Os registros das razões de terrígenos/Ca, Al/Ca, Ti/Al e Sr/Ca, sugerem uma tendência transgressiva para o topo da seção. Os padrões sedimentares de empilhamento e dados geoquímicos obtidos estão relacionados com eventos de ótimo climático ocorrido no Eoceno, que causou uma consequente subida relativa do nível do mar iniciado a aproximadamente 45 Ma.

APRESENTAÇÃO

Concentrações fossilíferas densas podem ser geradas através de três processos principais: a) sedimentológicos, b) biogênicos, e/ou c) diagenéticos (e.g., Kidwell et al., 1986). Concentrações densas apresentam padrões característicos relacionados aos processos envolvidos durante sua gênese (Brett and Baird, 1986; Speyer and Brett, 1986, Fürsich e Oschmann, 1993; Kidwell, 1986, 1991; Parras and Casadío, 2005; Mclaughlin and Brett, 2007; Brett, 2007; Conti et al., 2008; Dattilo et al., 2008, 2012; Hendy et al., 2009; Bressan and Palma, 2010; Zecchin and Catuneanu, 2013; Quaglio et al., 2014; Garcia-Ramos and Zuschin, 2019; Rigueti et al., 2020). Podendo fornecer informações paleoambientais e paleogeográficas, além de indicar mudanças relativas no nível do mar e superfícies estratigráficas (Brett e Baird, 1986; Speyer and Brett, 1986; Kidwell, 1991; Fürsich e Oschmann, 1993; Fürsich 1995; Abbott, 1997; Boyer et al., 2004; Holland, 2000, 2001; Tomašových, 2006; Puga-Bernabéu and Aguirre; 2017).

A Formação Man Aike, depositada durante o Eoceno-médio (45 Ma, George et al., 2020), tendo sido as dinâmicas ambientais, vigentes a sua sedimentação, atribuídas a variações climáticas regionais e globais (Miller and Gornitz, 2008; Ivany et al., 2008; Huyghe et al., 2012; Payros et al., 2012; Westerhold et al., 2017; Fosdick et al., 2020). No Vale do Rio de las Chinas, a base dos depósitos siliciclásticos marinhos do Eoceno médio representa como deposição em ambiente de *shoreface* superior formado em trato de sistema transgressivo (TST), com abundante fauna marinha (e.g., bivalves, briozoários, braquiópodes, dentes de tubarão e gastrópodes) e restos vegetais (ver Manríquez et al., 2019 para detalhes da flora).

Apesar de não haver um levantamento geocronológico da unidade ou de seu conteúdo fossilífero para a Formação Man Aike, ou ainda do significado dos acúmulos fossilíferos presentes nos depósitos Eocênicos da região do Vale do Rio de las Chinas, ela oferece uma oportunidade única de estudar os acúmulos fossilíferos gerados em uma bacia de antepaís de retroarco (*retroarc foreland basin*). O atual trabalho tem como objetivo compreender a gênese dos depósitos fossilíferos da Formação Man Aike, reconhecendo padrões que permitam correlacioná-los com variações de nível do mar e mudanças paleoclimáticas (regionais e globais) registradas durante o Eoceno.

Neste sentido, a hipótese apresentada nesse trabalho é de que as condições paleogeográficas, paleoclimáticas e mudanças relativas do nível do mar ocorridas durante o Eoceno Médio, registram assinaturas tafonômicas importantes para o reconhecimento

dos processos sedimentares, como camadas tempestíticas distais mais possantes e presença dominante de concentrações episódicas de fluxos de massa. Os resultados obtidos neste estudo foram submetidos ao periódico *Journal of South American Earth Sciences* conceito Qualis-CAPES B1.

1 **Genesis of dense shell accumulation of the middle Eocene Man Aike Formation**
2 **(Magallanes Foreland Basin, Chilean Patagonia).**

3

4 Eduardo Guareschi Müller^{1*}, Rodrigo Scalise Horodyski¹, Karlos Guilherme Diemer
5 Kochhann¹², Gerson Fauth¹², Leslie Marcela Elizabeth Manríquez¹³, Hugo Schimidt
6 Neto¹, Marcelo Adrian Leppe Cartes³.

7 ¹ Programa de Pós-Graduação em Geologia, Universidade do Vale do Rio dos Sinos,
8 Av. Unisinos 950, 93022- 000, São Leopoldo, Rio Grande do Sul, Brasil.

9 eduardoguareschi@hotmail.com, rhorodyski@unisinos.br, hugopaleo@hotmail.com

10 ² Itt Fossil- Instituto Tecnológico de Micropaleontologia, Universidade do Vale do Rio
11 dos Sinos, Av. UNISINOS, 950, 93022-000 São Leopoldo, RS, Brazil.

12 kkochhann@unisinos.br

13 ³ INACH- Laboratorio de Paleobiología Antártica y Patagonia, Instituto Antártico

14 Chileno, Plaza Muñoz Gamero, 1055, Punta Arenas, Chile. less.manriquez@gmail.com

15

16 *Corresponding author: Eduardo Guareschi Müller, eduardoguareschi@hotmail.com

17

18

19

20

21 **Highlights**

22 • Fossil accumulated as lag shell, hiatal, episodic and event
23 concentrations.

23

24 • Marine Eocene fossil accumulation in foreland basin

24

25 • Storm-influenced shallow marine siliciclastic deposits

25

26 **Abstract**

27 In El Puesto locality (Magallanes Basin, Chile), the Middle Eocene is represented
28 by coarse siliciclastic deposits interbedded with dense fossiliferous (shell-dominated)
29 accumulations of the Man Aike Formation. This study presents a multi-proxy
30 characterization of Man Aike Formation, based on facies, taphonomic and XRF (X-Ray
31 Fluorescence) analysis of bulk sediments. In the study area, the base of the sedimentary
32 succession is interpreted as transgressive facies stacking deposits in the shoreface zone.
33 Taphonomic signatures as articulation, fragmentation, dissolution and bioincrustation
34 suggests that shell accumulations are related to lag concentrations and mass flow started
35 by gravitational effects, influenced by weather- and storm-wave actions and currents.
36 Shell concentrations mostly characterize episodic deposits, which we interpret as
37 proximal and distal tempestites. Lowest shell concentrations are interpreted as
38 fossiliferous lags, suggesting the onset of the transgression in the Magallanes Basin.
39 Shelly deposits composed of closed and articulated bivalves, observed in the middle
40 portion of succession, were interpreted as episodic generated by mass flow deposits. In
41 the middle-upper portion a hiatal concentration followed by an event concentration is
42 observed, marked by abrupt deposits of articulated and concordant shell. Results of
43 geochemical analyses (terrigenous elements/Ca, Al/Ca, Ti/Al and Sr/Ca ratios) support
44 the interpretation of a deepening trend upward for the sedimentary succession. The results
45 observed in this study is related to warming events of the middle Eocene, and influence
46 of the regional tectonic activity (Drake Straight opening).

47

48 **Keywords:** Taphonomy, geochemistry, shell concentrations, retroarc foreland deposits,
49 Eocene warming events.

50

51 **1. Introduction**

52

53 Dense accumulations (or concentrations) of biologic hard parts, more than 2 mm
54 in size, irrespective of taxonomic composition, state of preservation, or degree of post-
55 mortem modification are generally defined as skeletal (or fossil) concentrations (sensu
56 Kidwell, 1986; Kidwell and Holland, 1991). They provide critical data for sedimentary
57 and stratigraphic analyses in siliciclastic successions (Kidwell et al., 1986; Beckvar and
58 Kidwell, 1988; Simões and Kowalewski, 1998; Parras and Casadío, 2005; Hendy et al.,
59 2006; Patzkowsky and Holland., 2012; Zecchin and Catuneanu, 2013; Garcia-Ramos and
60 Zuschin, 2019).

61 Skeletal concentrations can be formed during intervals of sediment starvation,
62 winnowing, dynamic bypassing and/or erosional reworking under specific energy
63 conditions, or by increased input of bioclast (Brett and Baird, 1986; Kidwell, 1986;
64 Kidwell et al., 1986; Beckvar and Kidwell, 1988; Kidwell, 1989; Fürsich and Oschmann,
65 1993; Simões and Kowalewski, 1998; Bressan and Palma, 2010; Hendy et al 2006; Fick
66 et al., 2018; Rigueti et al., 2020). In this sense, such concentrations provide significant
67 information about important stratigraphic boundaries in sequences (e.g., Banerjee and
68 Kidwell, 1991; Brett, 1995; Holland, 1995; Abbott, 1997; Holland, 2000; Holland, 2001;
69 Fürsich and Pandey, 2003; Parras and Casadío, 2005; Holz and Simões, 2005;
70 Tomašových, 2006; Hendy et al., 2009; Zabini et al., 2012; Puga-Bernabéu and Aguirre,
71 2017; Garcia-Ramos and Zuschin, 2019), storms effects, biological interaction and
72 energy dissipation in shallow marine environments, also provide paleoenvironmental
73 features about paleogeography configuration and costal profile (e.g., Speyer and Brett,
74 1986; Kidwell, 1990; Fürsich and Oschmann, 1993; Fürsich, 1995; Kidwell and
75 Brenchley, 1994; Boyer et al., 2004; Tomašových, 2006; Schmidt-Neto et al., 2018a,b).

76 Changes in the sedimentary regime, hydrodynamic processes related to storm
77 events and relative sea level changes creates unique taphonomic patterns in dense fossil
78 accumulation, and is used to infer the input of hardparts, cyclicity in accumulation
79 patterns, and environmental energy (Kidwell et al., 1986; Kidwell, 1986, 1991; Speyer
80 and Brett, 1986, 1988; Miller et al., 1988; Davies et al., 1989; Holland, 1995; Myrow,
81 2005; Dattilo et al., 2008, 2012; Quaglio, et al., 2014; Puga-Bernabéu and Aguirre, 2017;
82 Fick et al., 2018; Rigueti et al., 2020). The geometry of the deposits is also used to
83 distinguish environmental characteristics and dynamics, such as energy regimes,
84 paleogeographic characteristics, sedimentation rates, and water oxygenation (Kidwell et
85 al., 1986; Brett and Baird, 1986; Fürsich and Oschmann, 1993; Schmidt-Neto et al.,
86 2018).

87 Relative sea level changes, kinetic potential, sedimentation rate, and
88 geomorphology have been recognized as the main controlling factors on the geneses of
89 dense fossiliferous deposits (Brett and Baird, 1986; Speyer and Brett, 1986; Fürsich and
90 Oschmann, 1993; Brett et al., 2007; McLaughlin and Brett, 2007; Hendy et al., 2009;
91 Zecchin and Catuneanu, 2013; Horodyski et al., 2019; Erthal and Ritter, 2020; Rigueti et
92 al., 2020). Therefore, it is crucial to integrate paleogeographic and paleoenvironmental
93 reconstruction, as well as sedimentary and petrographic analyses, to improve our
94 understanding about the genesis of fossiliferous accumulations (Shoup, 2001; Simões and
95 Torello, 2003; Bressan and Palma, 2010; Quaglio et al., 2014; Samira et al., 2018; Garcia-
96 Ramos and Zuschin, 2019; Chinellato et al., 2020; Erthal and Ritter, 2020; Rigueti et al.,
97 2020).

98 The Magallanes Basin offers an unique opportunity to understand the processes
99 that influenced the deposition of dense fossiliferous concentrations accumulated in a
100 retroarc foreland basin, displaying a large continuous side and vertical succession. The

101 foreland basin paleogeographic setting during the Eocene developed a unprotected coast
102 subject to high energy depositional processes and transgressive-regressive events
103 (Marensi et al., 2002; Nullo et al., 2006; Manríquez et al., 2019). Moreover, shallow
104 marine sediments generated in a foreland basin tend to experience the effects of storms
105 events and currents more effectively. Due the lack of taphonomic studies in retroarc
106 foreland basins, and the genesis nature, the objective is understand the genesis of dense
107 marine fossiliferous accumulations of the Man Aike Formation, as well as and their
108 environmental and climatic significance during the Middle Eocene (Lutetian).

109

110 **2. Geological Settings**

111

112 The Magallanes/Austral Basin (MAB) is a north-south elongated retroarc foreland
113 basin, covering the southern regions of Chile and Argentina (Figure 1). The MAB
114 emplacement was related with the Late Cretaceous to Neogene uplift of the southern
115 Andean orogen (Wilson, 1991; Fildani et al., 2008; Fosdick et al., 2011; Fosdick et al.,
116 2020; Daniels et al., 2018). This retro-arc foreland basin recorded Early Cretaceous to
117 Miocene paleoenvironmental changes that occurred in high southern paleolatitude, after
118 the break-up of Gondwana (Mella, 2001; Manríquez et al., 2019; Sames, 2020).

119

120 *Figure 1*

121

122 During the Cretaceous, the Magallanes region (Chile) was subject to deformation
123 of the Pacific margin, product of a compressive regime associated with the rupture of
124 Gondwana and the opening of the Atlantic Ocean (Biddle et al., 1986; Harambour and
125 Soffia, 1988; Mella, 2001). This geological event was responsible for generating a flexure

126 deformation giving rise to the foreland Magallanes/Austral Basin (Natland et al., 1974;
127 Wilson, 1991; Fildani et al., 2003; Malkowski et al., 2017).

128 The sedimentary succession of Magallanes Basin is composed of Upper
129 Cretaceous to middle Paleogene deposits. During the Late Cretaceous (Campanian Age)
130 the sedimentary environment was characterized by a high relief shelf and slope system
131 (Tres Pasos Formation) (Shultz et al., 2005; Romans et al., 2011; Schawartz and Graham
132 2015; Auchter et al., 2016; Manríquez et al 2019). Shallow marine and deltaic deposits
133 (Dorotea Formation) recorded the boundary between Late Cretaceous (Campanian-
134 Maastrichtian) and the early Paleogene (Romans et al., 2011; Gutiérrez et al, 2017;
135 Daniels et al., 2018; George et al., 2020). Fluvial, deltaic, marine, and tide deposits
136 represent the Dorotea Formation in northern sector of the Rio de las Chinas Valley (Vogh
137 et al. 2014; Schwartz and Graham, 2015; Manríquez et al., 2019). These deposits contain
138 invertebrates, plant impressions and vertebrate remains (Manríquez et al., 2019; Alarcón-
139 Muñoz et al., 2020; Goin et al., 2020; Martinelli et al., 2021). Finally, during the middle
140 Paleogene (Lutetian-Bartonian) shallow marine and estuarine facies were deposited,
141 characterizing the Man Aike Formation (Malumián, 1990; Camacho et al., 2000;
142 Marensi et al., 2002; Nullo and Combina, 2011). The Man Aike Formation is interpreted
143 to record the drowning of continental areas within a transgressive systems tract
144 (Malumián, 1990; Camacho et al., 2000; Marensi et al., 2002; Manríquez et al., 2019).
145 At the study area, abundant marine fauna (bivalves, bryozoans, brachiopods, shark teeth
146 and gastropods) and wood debris occur (Manríquez et al., 2019). In El Puesto locality,
147 the maximum depositional age for the lowermost portion of the Man Aike Formation date
148 from 45.7 ± 0.6 Ma (middle Eocene) based on detrital U-Pb zircon (George et al., 2020).

149 Several studies recognized a Paleocene unconformity at the base of the Man Aike
150 Formation, expressed by ~ 20 Myr hiatus (Casadio et al., 2009; Vogt et al., 2014; Gutierrez

151 et al., 2017; Schwartz et al., 2016; Daniels et al., 2018 George et al., 2020; Manríquez et
152 al., 2019). This widespread erosion is interpreted as a consequence of the Paleocene uplift
153 of the Patagonian Andes (e.g Biddle et al., 1986; Malumian et al., 1996; Kraemer et al.,
154 2002; Ramos, 2002; Fosdick et al., 2015a; Fosdick et al., 2015b; George et al., 2020;
155 Rivera et al., 2020). In the Rio de las Chinas Valley, Manríquez et al., (2019) interpreted
156 that the base of the Man Aike Formation recorded a shoreface environment formed during
157 a transgressive systems tract (TST), associated with a minor order retrogradational
158 stacking overprinted by an aggradational stacking of higher order.

159 This formation is interpreted in other localities as shallow marine to estuarine
160 deposits, dating from middle to upper Eocene (Casadío et al., 2009; Le Roux et al., 2010;
161 Ugalde, 2014; Gutiérrez et al., 2017). In the El Calafate region (Argentina) is interpreted
162 as infill of incised valleys during a transgressive period, composed of conglomerates and
163 sandstones intercalated with coal layers, with fossil content composed of marine
164 invertebrates and wood debris (Marensi et al., 2002, 2003). The Man Aike Formation
165 has been correlated with Río Turbio Formation (Figure 2) (Malumián and Caramés, 1997;
166 Malumián and Panza., 2000; Pearson et al., 2012; Fosdick et al., 2015; Fosdick et al.,
167 2020).

168

169

170

171 *Figure 2*

172

173

174

175

176 3. Materials and Methods

177

178 Sedimentological and paleontological studies were developed during the Chilean
179 Antarctic Institute (INACH) expedition carried out in the summer season of 2020. Three
180 sections have been described in the middle Eocene deposits of the Man Aike Formation,
181 at the Rio de las Chinas Valley. The main profile (Profile 1) was complemented by data
182 from other two profiles and unified in a composite profile (Figure 3).

183 Fieldwork consisted in descriptions of sedimentary facies with stratigraphic
184 control, dense fossil concentrations and taphonomic signatures. Codes for sedimentary
185 facies were adapted from Miall (1996). Deposits with significant fossil accumulations
186 (above 10% of the volume of the deposit composed of bioclasts) were classified as hybrid
187 facies (sensu Mount, 1985; see Kern et al., 2019). For hybrid facies the letter ‘H’ was
188 employed at the beginning of the code, characterizing a fossil accumulation in siliciclastic
189 rocks. Our sedimentologic description took into account thickness, geometry and lateral
190 extent of strata, bedding plane features, packing of shells, matrix, trace fossils, and
191 sedimentary structures.

192 In the taphonomic analysis, we adopted the conceptual framework for field
193 description of dense fossil concentrations proposed by Kidwell and Holland (1991).
194 Paleoenvironmental and biostratigraphic interpretations follow Brett (1990), Brett (1995),
195 Brett and Baird (1986), Fürsich and Oschmann (1993) and Speyer and Brett (1988). Our
196 taphonomic descriptions applied qualitative criteria taking into account: a) geometry; b)
197 packing of bioclasts: dense/loose/disperse; c) taxonomic composition; d) size-sorting of
198 bioclasts: well sorted / moderated sorted / poorly sorted; d) type of matrix for bioclasts
199 greater than 2 mm in diameter (Kidwell et al., 1986; Kidwell and Holland, 1991).
200 Taphonomic features like orientation in plan-view, orientation in cross section

201 (concordant / perpendicular / oblique), degree of articulation (high / moderate / low),
202 fragmentation degree (high / moderate / low), bioencrustation / bioerosion, and corrosion
203 (sensu Brett and Baird, 1986) were observed.

204 Three distinct hybrid facies were described from five (5) fossiliferous
205 accumulations. Five (5) samples were collected from the skeletal accumulations to carry
206 out thin section petrographic descriptions. Petrographic analysis was performed with a
207 ZEISS AXIO optical microscope at UNISINOS University. We follow criteria by
208 Dickinson (1885) and Folk (1980) for describing fossil-bearing rocks.

209

210 *Figure 3*

211

212 3.1 X-Ray Fluorescence (XRF) analysis

213 Environmental interpretations were complemented with geochemical analyses of
214 32 unaltered rock samples collected at a stratigraphic resolution of 1 m. Intensities of both
215 major and trace elements were measured on the bulk sediment samples using an Epsilon
216 1/PanAlytical XRF spectrometer at itt Fossil (UNISINOS University). Measurements
217 were performed on 10 g of loose powder samples (previously ground and dried) using the
218 same settings described by Krahl et al. (2020). Results were expressed in counts per
219 second (cps) and the main elemental ratios utilized in this work are summarized in the
220 Table 1.

221

222

223 *Table 1*

224

225

226 **4. Results and Interpretation**

227

228 4.1 Lithofacies and Facies Association

229

230 The Eocene sedimentary succession in the study area reach ~32 m thick, displaying
231 a continuous sedimentary (Figure 4). These deposits are represented by conglomerates
232 and medium to very-coarse grained sandstones interbedded with fossiliferous
233 accumulations. The sedimentary facies were divided into five (5) siliciclastic facies and
234 three (3) hybrid facies with marine fossils (Figure 5). These facies reach kilometers of
235 lateral expression. In Man Aike Formation are recognized facies associations related to
236 upper shoreface, middle shoreface, and lower shoreface (Table 2).

237

238 *Figure 4*

239

240 *Figure 5*

241

242 *Tabela 2*

243

244 4.1.1 – Upper Shoreface facies association

245

246 This facies association comprise ~17 m thick interval, occurring in the lowest
247 portion of the sedimentary succession encompasses four siliciclastic facies (Gmg, St, Sp,
248 Sm) and one hybrid facies (Hsm) (Table 2, Figure 6). The conglomerate facies (Gmg)
249 varies between 0.5 and 3 m in thickness, and presents hundreds of meters of lateral
250 extension. The Gmg facies is characterized as a matrix to clast-supported conglomerate

251 with inverse grading, diffuse trough cross-bedding and scattered bioclasts and wood fossil
252 (Figure 6 A).

253 The sandstones facies are represented by tabular beds composed of coarse-grained
254 massive sandstones (Sm facies), sandstones with dispersed pebbles and granules with
255 medium to large scale planar through cross-bedding (Sp facies), lenticular co-set beds
256 composed of medium to coarse-grained sandstones, and laterally continuous beds
257 composed of medium to very coarse-grained sandstone with small to medium-scale
258 trough cross -bedding (St facies) (Figure 6 A, B, C, E, F). These facies can reach up to 2
259 m in thickness and tens of meters in lateral extension (Figure 6 G).

260 Hybrid facies are represented by two centimetric to metric beds (Hsm facies)
261 (Figure 6 C, D). These beds display pebbly massive coarse-grained sandstones with
262 hundreds of meters of laterally extension, ranging from 0.5 to 1.5 m thickness, with
263 irregular and erosive basal boundaries, and are vertically associated with the Sp and Sm
264 facies. Fossil accumulations show polytypic assemblages with bimodally sorted bioclasts,
265 varying from loose to densely packed, with bioclasts in concordant to oblique position in
266 relation to the bedding plane. The biofabric is internally complex and composed of an
267 allochthonous assemblage of articulated and disarticulated shells (Pectinids and *Lahillia*).

268

269 4.1.1.1 Interpretation

270

271 The proximal setting within the studied sequence is expressed by the basal Gmg
272 facies, showing signs of grain shock (inverse grading) as the result of dune bedload
273 migration under unidirectional traction flow, generating 3D-dunes (see Dasgupta and
274 Manna, 2011). The Sp and St facies represent the migration of straight and sinuous crested
275 dunes, respectively. In this sense, the Gmg St and Sp facies were related to upper

276 shoreface deposits generated by coastal drift currents (Harms et al., 1982; McCubbin,
277 1982; Hart and Plint, 1989; Johnson and Baldwin, 1996; Reading and Collinson, 1996).

278 The Sm facies, represented by massive sandstones beds, was likely deposited
279 during high sedimentary discharge periods (Rossi et al., 2016) or affected by post-
280 depositional fluidization process (De Souza et al., 2019). Finally, the hybrid facies (Hsm)
281 represented by extensive beds is interpreted as fossiliferous lags formed during high
282 frequency transgressive pulses, suggesting a wave-ravinement surface (Kidwell et al.,
283 1986; Kidwell 1989; Cattaneo and Steel, 2003; Fursich and Oschmann, 1993; Hendy et
284 al., 2006; Yang, 2007; Alván and Von Eynatten, 2014; Zecchin and Catuneanu, 2012;
285 Zecchin et al., 2017; Kern et al., 2019).

286

287 *Figure 6*

288

289 4.1.2 – Middle-Lower shoreface facies association

290

291 This facies association occurs on the upper portion of the study area and
292 encompasses one siliciclastic facies (Scs) and two hybrid facies (Hgm_g and Hgm_m)
293 (Table 2, Figure 7). The Scs facies is represented by amalgamated swaley cross-stratified
294 sandstones varying from 2 to 6 m in thickness and hundreds of meters of lateral extension
295 (Figure 7A). Interbedded with these sandstones, there are lenticular and wedge-shaped
296 gravelly sandstones ranging from 0.5 to 5 m in thickness and extending laterally for tens
297 to hundreds of meters. Sparse burrows represented by *Skolithos* and *Thalassinoides* are
298 observed at the base of the Scs facies that rests over the hybrid facies (Supplementary
299 Figure S1). Subordinated hummocky cross-stratifications were also noted
300 (Supplementary Figure S2 G).

301 *Thalassinoides* subvertical burrows show bifurcation and compactation, with
302 passive infilling of the burrow (intergrowing of carbonate mineral) (Supplementary
303 Figure S1 D). Finally, *Skolithos* vertical burrows, active infill (material similar to the
304 surrounding matrix) with sizes about 5 to 20 cm (Supplementary Figure S1 A, B, C).

305 The hybrid facies include gravelly sandstones wedges, grading from gravel to
306 coarse-grained sandstones, with increase of sand matrix upward and decrease of gravel
307 and pebble (Hgm_g facies, Table2) (Figure 7 C, D). Also, lenses of massive pebble
308 sandstones with inverse graded bioclasts, with decrease of matrix content upward and
309 increasing in close-packing is noted (Hgm_m facies, Table 2) (Figure 7 B).

310 The Hgm_g facies is represented by wedge-shaped gravelly sandstones, ranging
311 between 0.5 and 6 m in thickness and hundreds of meters of lateral extension, being often
312 interbed with S_{cs} facies (Figure 7 C, D). These deposits are bounded by erosive surfaces
313 at the base and the top. The lower portion of the beds show a gravel lithology with normal
314 gradation, and coarse bioclasts concentration arranged in lenticular shell accumulations
315 (Supplementary Figure S2 A, C). The intermediate portion characterized by gravel
316 deposits with sand-rich matrix and dispersed packed bioclasts, grading laterally from
317 massive to planar bedding. Finally, the uppermost portion of these deposits is represented
318 by medium to coarse-grained massive sandstones and show dispersedly packed bioclasts.
319 Punctual occurrences of open-articulated valves have been observed in the shell
320 concentrations of the uppermost interval (Supplementary Figure S2 D).

321 The Hgm_m facies occurs as a punctual laterally discontinuous lens, ranging from
322 0.5 to 2 m in thickness, and extending laterally for tens of meters (Supplementary Figure
323 7 B). The Hgm_m facies contains polytypic assemblages, complex internal concentrations
324 of articulated and disarticulated shells with an increasing upward trend of close-packing
325 (Figure 7 B). Punctual pavements occur in the uppermost portion of beds, usually showing

326 closed and concretionary shells (Supplementary Figure S2 B, D, E). The Hgmm facies
327 occurs interbedded with the Scs and Hgmg facies.

328

329 4.1.2.1 Interpretation

330

331 The swaley cross-stratification is assigned to be formed under storm waves by
332 oscillatory high-energy combined-flow regime (Duke, 1985; Dumas and Arnott, 2006).
333 Dumas and Arnott (2006) hypothesized that swaley cross-stratification tend to be
334 deposited by an aggrading hummocky bed between fair-weather and storm wave base,
335 however, in shallower water where aggradation rates are low enough to cause preferential
336 preservation of swales. Therefore, these mud-free swaley cross-stratification deposits are
337 interpreted as middle shoreface tempestite deposits (Aigner and Reineck, 1982; Aigner,
338 1985; Seilacher and Aigner, 1991; Plint, 2010). The middle shoreface usually is strongly
339 influenced by oscillatory wave energy, storms waves and currents (Leckie and Walker,
340 1982; Pemberton et al., 2012).

341 *Thalassinoides* and *Skolithos* are preserved under low densities, only in the
342 lowermost portion of the bed. These ichnofossils normally indicate the boundary between
343 the lower and middle shoreface, represent by the presence of suites to those that
344 correspond to the *Skolithos* Ichnofacies (MacEachern and Pemberton, 1992; MacEachern
345 et al., 1999b; Peberton et al., 2001; 2004; 2012). *Thalassinoides* could point the change
346 in the consistence of substrate that became more plastic and consistent than shallower
347 portions (Bromley, 1996). Overall, the occurrence of these trace-fossils in amalgamated
348 tempestites (swaley cross stratified sandstones) are indicative of storm-dominated
349 systems, usually assigned to middle shoreface (e.g., Greenwood and Sherman, 1986;
350 Dumas and Arnott, 2006; Pemberton et al., 2012; Maahs et al., 2019).

351 The Hgmg facies, which occurs interbedded with the sandstones with swaley
352 cross-stratification, is interpreted as the result of gravitational concentrated (granular)
353 flows characterized by dispersive pressure, normally associated with steep slopes (see
354 Zavala, 2020). In this case, the sedimentation from the incipient basal granular mass flow
355 decanted due to loss of flow capacity (Lowe, 1979, 1982; Manville and White, 2003;
356 Zavala et al., 2011, 2014). Imbricated shells in the lowermost portion of the beds within
357 the gravel fraction is indicative of unidirectional flows and tractive processes, which were
358 able to carry shells into the low cohesiveness matrix (sandy matrix). These concentrated
359 granular flows have low capacity to transport heavy particles over long distances and
360 require steep slopes to accelerate (Dasgupta, 2003; Manville and White, 2003; Zavala et
361 al., 2011, 2014; Conti et al., 2019; Zavala, 2020).

362 These graded beds are consistent with non-cohesive flows, here is interpreted as
363 concentrated granular flows (e. g., Zavala 2020). This type of sedimentary gravity flow
364 was previously classified as grain flows (see Lowe, 1979; Lowe, 1982) or cohesionless
365 debris flows (*sensu* Nemeč and Steel, 1984). According to Zavala (2020), when the fast-
366 moving inertia flow stops, the slower moving segregated suspension cloud bypasses the
367 coarse-grained concentrated flow deposits, sometimes showing lens-shaped sand bodies
368 and often exhibiting cross-bedding.

369 The Hgmm facies is represented by lenticular beds interspersed between the
370 Hgmg and the Scs facies, along with glauconite, and *Thalassinoides* passively filled with
371 well-formed calcite minerals by precipitation. Cohesive unconsolidated sediments are
372 necessary to formation of *Thalassinoides* isp. suggesting distal zones near to the slope. In
373 this sense, the Hgmm facies is interpreted as deposits distal zones of the middle shoreface,
374 while the top of the sequence would be have been deposited between fair-weather and
375 storm-wave base levels. Pavements with bioclast randomly distributed, on the upper

376 erosive contact, associated with swaley cross-stratified beds, point a zone with dynamic-
377 bypass process triggered by storm events (see Kidwell 1986; Miller et al., 1988; Dattilo
378 et al., 2008, 2012; Fick et al., 2018).

379

380 *Figure 7*

381

382 4.2 X-ray fluorescence (XRF) and Petrography analysis

383

384 The terrigenous/Ca and Al/Ca ratios were used to infer terrigenous input and
385 runoff intensity (Beil et al., 2018; Spofforth et al., 2008). Both ratios depict overall
386 decreasing-upward trends within the studied succession, with markedly low values within
387 the shell beds at 4 and 6 m (Figure 8 A, B).

388 The Ti/Al ratio is used to infer environmental energy and proximity to the source
389 area (Bourget et al., 2008; Spofforth et al., 2008; Kwiecien et al., 2009; Berg et al., 2010;
390 Henrich et al., 2010; Chen et al., 2013). This ratio presents peaks within the lowermost
391 10 m of the studied succession and decreases upward (Figure 8 C).

392 High Sr/Ca ratios are usually associated with precipitation of authigenic
393 carbonates at shallow marine settings (Rothwell et al., 2006; Thomson et al., 2006; Grove
394 et al., 2010). Within the studied succession, the Sr/Ca ratio is high from 0 to 15 m and
395 decreases upward. (Figure 8 D).

396 The Log (Zr/Rb) ratio has been used as a sediment grain-size and high energy
397 process proxy in marine environments (Dypvik and Harris, 2001; Rothwell et al., 2006;
398 Wang et al., 2001). Within the studied succession, the Log (Zr/Rb) presents marked peaks
399 and high values within the lowermost 15 m of the studied succession and a well-marked
400 decreasing upward trend (Figure 8 E).

401

402 *Figure 8*

403

404 Petrographic analyses of selected samples enabled us to identify immature pebble
405 and gravel bearing sandstones, with carbonate and ferric cementation, and high amount
406 of glauconite (Supplementary Figure S3 B). Heavy minerals increase in relative
407 abundances in the Hsm facies. Calcite cement is present throughout the interval not being
408 restricted to the fossil and shell bearing rocks, as observed in the field due to the reaction
409 of rocks with a weak HCl solution. Therefore, all samples are identified as sublitharenite
410 according to Folk (1980). In general, the grain size is coarse along the sequence, with
411 total absence of claystones and siltstones. Therefore, low values of Log (Zr/Rb) within
412 lowermost 10 m of the sequence probably reflect a “clay effect” caused by the presence
413 of high amount of glauconite in these beds (see Kennedy, 2015).

414 In general, samples show high amount of volcanic, metamorphic, and sedimentary
415 grains, indicating low mineralogical and textural maturity and proximity to source areas
416 (Dickinson, 1980). Despite incipient dissolution can be found in feldspar grains, K-
417 feldspar and plagioclase grains with twinning and well-preserved volcanic grains were
418 also found indicating an immature and mixed sedimentary source (Supplementary Figure
419 S3 A). Grains are overall well-preserved, showing only incipient dissolution. Glauconite
420 is present in major quantities in the lowermost part of the sequence associated with Hsm
421 facies (Supplementary Figure S3 B), and in less quantity through the top (Hgmm facies).
422 Low compaction is indicated by predominant punctual and subordinated concave-convex
423 grain contacts (Supplementary Figure S3 C). Bioclasts normally show silicification, well-
424 preserved structures, and are infilled by the sedimentary matrix (Supplementary Figure

425 S3 D, G, H). The primary detrital composition is similar in all fossil concentrations,
426 suggesting a conservative provenance (see Dickinson, 1985; Weltje and Evhatten, 2004).

427

428 4.3 Taphonomic Description of Fossil Concentrations

429

430 Five densely packed fossil concentrations preserved in a siliciclastic matrix were
431 described to Man Aike Formation. All fossil material found along the succession were
432 classified as bivalved shells (Bivalvia), univalved shells (Gastropod) and multi-element
433 skeletons (Bryozoan) (Supplementary Figure S2).

434 Three genetic types of fossil concentrations were identified and are detailed
435 below. For the genetic classification, biofabric, geometry and lateral distribution was
436 considered, as well the biostratigraphic features. The fossil concentrations are coded as 1-
437 3, relative to the stratigraphic position of the succession.

438

439 4.3.1 Fossil concentration 1 - Facies Hsm (Figure 9)

440

441 This fossil concentration is preserved as the Hsm facies, and occurs as two 0.2-
442 0.3 m thick beds positioned at 2 and 5 m within Profile 1. This levels are laterally
443 correlated with the shell bed observed at 6 m (1.5 m thick) in supplementary Profile 2
444 (Figure 3), and are laterally continuous for hundreds of meters (Figure 9 A). The close-
445 packing degree of fossils is classified as loose to densely packed (25% - 50%). Coarse
446 siliciclastic grains characterize the matrix, being poorly sorted and ranging in size from
447 coarse sand to pebble with low compositional maturity (Supplementary Figure S3 A, C).
448 Glauconite grains and calcite cementation is verified in thin section (Supplementary
449 Figure S3 B). Bivalved-type skeletons *Lahillia* sp. and pectinids (Figure 9 B, D and E)

450 are present. Bioclasts displays bimodal size-sorting with pectinids ranging in size from 2
451 to 3 cm, associated with the *Lahillia* ranging in size from 7 to 9 cm.

452 Bioclasts show concordant preferential orientation in cross-section, with
453 subordinated shells in perpendicular position related to the bedding planes.
454 Predominantly, convex-down shell positions were noted (Figure 9 D). Despite the fact
455 that few bivalves have been preserved articulated, the majority was preserved
456 disarticulated whole shell (Figure 9 B, E). Moderate degree of abrasion and high degree
457 of disarticulation also were observed. No bioerosion and encrustation were observed.

458

459 *Figure 9*

460

461 4.3.1.1 Interpretation

462

463 Taphonomic characteristics of these concentration, such as different degrees of
464 completeness, abrasion, rare articulated shells, and convex-down shells suggest the
465 bioclasts were subject to reworking generated by currents or waves. The lack of bioeroded
466 and encrusted shells suggest low periods of exposure in the sediment/water interface. In
467 this sense, the taphonomic damage observed have been generated in a proximal
468 environment, under moderate to high energy conditions, and having been subjected to
469 repeated exhumation and burial processes generated by waves and currents. As a
470 consequence, hydraulic and biogenic amalgamation of many different generations are
471 observed in these deposits.

472 Fossil concentrations formed during transgressive pulses tend to show reworking
473 of buried shells and clasts, well preserved shells along with poorly preserved, mostly
474 concordant, relative wide lateral distribution, and erosive contacts (e.g., Kidwell et al.,

475 1986; Cattaneo and Steel, 2003, Yang, 2007). These taphonomic features are interpreted
476 as signatures of sedimentary environments close to the fair-weather wave base (Alván
477 and Von Eynatten, 2014). According to Einsele (2000), proximal tempestites with highly
478 erosive bases are formed in the middle shoreface, and their occurrence is rare in the upper
479 shoreface.

480 High energy events like storms tend to cause high sedimentation rates, preventing
481 reworking and exposure of bioclasts, and reducing physical damages on shell, after
482 reworked by transgressive pulses (e.g., Anderson and McBride 1996; Schmidt-Neto et
483 al., 2018). Additionally, changes in sedimentation tend to be more accentuated in gravel-
484 dominated shallow marine transgressive successions (Clifton, 2003).

485 Gutter cast are common features on these beds (Facies Hsm). According to Tucker
486 (2001), gutter casts are typically associate with shallow marine sediments under storms
487 currents, corroborating our interpretations that the fossil concentrations were subject to
488 storm-related processes during their genesis. On the other hand, the bulk of the coarse-
489 grained lithologies represents amalgamated proximal lag-type tempestites containing
490 reworked shells and glauconite grains, pointing to quiescent periods (Engelbrecht, 2000).

491

492 4.3.2 Fossil concentration 2 -Facies Hgmg (Figure 10)

493

494 Fossil concentration 2 is preserved within the Hgmg facies. They are expressed as
495 wedges-shaped gravelly sandstone bedforms at the mid-upper portion of Profile 1,
496 between 19 and 22 m, and at 32 m. They are laterally correlated with Profile 3 (Figure 3).
497 These fossil concentrations are expressed as boxed-up lens concentration, a couple of
498 meters wide and thicknesses ranging from 0.5 to 1 m. Locally distributed in the lowermost

499 part of the beds, displaying erosive boundaries with the Scs facies below (Figure 10 A,
500 B, C). Localized gradational upper boundary, associated with Hgmm facies, was noted.

501 Close-packing degree ranges from loosely to densely packed (25% to >75%),
502 decreasing upward within the beds. Matrix is characterized by gravelly sandstones, with
503 grain sizes ranging from coarse sand to cobble size with subangular to subrounded
504 granules and pebbles of polymictic fragments (gneiss, schist, granite, quartz, bioclast and
505 feldspars), and silicified bioclast (Supplementary Figure S3 G, H). Bioclasts are poorly
506 sorted with pectinids ranging from 2 to 10 cm in size. This concentration contains well
507 preserved fossils, identified as *Lahillia*, *Venericardia*, *Ostrea*, and bryozoan and bivalve
508 casts (Figure 10 E) (Supplementary Figure S2 A, C, F). Bryozoans are loose in the matrix,
509 no incrustated in the shells.

510 Bioclasts are randomly oriented in plain view, and occur in obliquely and/or
511 vertical position in relation to the bedding plane, with subordinated concordant
512 orientation. Occurrence of shells disposed in preferential convex-down position is
513 predominant. Also, open-articulated *Lahillia* with no preferential orientation and locally
514 distributed were observed (Supplementary Figure S2 D). Despite the occurrence of
515 bivalve fragments, most fossils were preserved as whole shells. Articulated and disjointed
516 shells are present (Figure 10 B, C, D). In the lower portion of the beds, locally distributed
517 bioclast-supported lens displays imbricated disarticulated shells, as well as clustering
518 patterns like imbrication, staking and edgewise (Figure 10 B, C) (Supplementary Figure
519 S2 C). No abrasion and bioerosion were observed.

520

521 *Figure 10*

522

523 4.3.2.1 Interpretation

524

525 Shell's box-up lenses in the lowermost part of the bed, often with oblique and
526 perpendicular orientation of shells suggest extraordinary depositional processes like
527 debris flows (Speyer and Brett, 1986, 1988). Taphonomic signatures that indicates a
528 rapid-burial of shell includes low degree of fragmentation, abrasion, and preservation of
529 articulated shells in life orientation (Speyer and Brett, 1986; 1988; Kidwell; 1991; Shoup,
530 2001; Hendy et al., 2006).

531 The nested and stacked disarticulated bivalves point to high amounts of bioclasts
532 available in the environment, as well as their deposition by high energy events like high-
533 density turbulent flows (e.g., Middleton, 1967; Fürsich and Oschmann, 1986, 1993;
534 Kidwell and Bosence, 1991; Kidwell and Holland, 1991; Simões et al., 1996).
535 Furthermore, grouping of bioclasts forming clustering patterns, such as imbrication and
536 stacking, is probably the result of shell/shell interferences (see Futterer, 1978).

537 These fossil concentrations are distributed in these gravelly subaqueous debris
538 deposits as product of tractive flow of sediment-laden water with dispersive pressures,
539 which graded the matrix by grain size (Lewis et al., 1980; Lowe, 1979, 1982; Nemeč and
540 Steel, 1984; Miall, 2006; Zavala, 2020). These shell concentrations represent episodic
541 deposits formed by rapid burial generated by debris flows (Kidwell, 1991; Hendy et al.,
542 2006; Garcia-Ramos et al., 2020; Quaglio et al., 2014). This kind of shell concentration
543 reflects deposits generated on high gradient slope areas (Conti et al., 2009; Quaglio et al.,
544 2014; Zavala et al., 2011; 2014; Zavala, 2020). The lateral interdigitation of these deposits
545 (Facies Hgmg) with Scs facies, is an indicative for storm-influenced depositional settings
546 in the middle shoreface (Myrow, 2005).

547

548

4.3.3 Fossil concentration 3 - Facies Hgmm (Figure 11)

This fossil concentration is preserved within the Hgmm facies, expressed as thin lenticular laterally discontinuous (tens of meters long) beds, ranging from 0.15 to 1.20 m in thickness, and occurring at 27 m in Profile 1 and at 1 to 7 m in the Profile 3 (Figure 3). The lower boundary is gradational while the upper boundary is erosive. The Scs facies display an erosional basal contact with these beds (Figure 11 A).

Upward, the packing degree of bioclasts increases (15%-50%) (Figure 11 A, C). Matrix is characterized by pebbly sandstones with coarse bioclasts. Volcanic and metamorphic siliciclastic grains like gneiss, schist, granite, quartzite, and feldspar are identified in the rock (Supplementary Figure S3 D, E, F). Glauconite grains and carbonate cementation is noted. Bivalve-type skeletons and univalve-type skeletons occur (Figure 11 B, D). The fossils are mainly preserved as replaced silicified shells (Supplementary Figure S3 D). Bioclasts sizes range between 2 and 8 (cm).

Bioclasts are disposed randomly in the plane view (Figure 11 B, C, D). Broken shells of pectinids and gastropods are dominant. Despite few bivalves have been preserved articulated (at the top boundary of the beds), the majority was preserved disjointed, and varying from moderated to highly fragmented shells (Figure 11 B, C). Articulated bivalves, in oblique and perpendicular position relative to the bedding plane was noted on the top of the beds, mostly in concretions (Figure 11A, E) (Supplementary Figure S2 E). Moderate dissolution and abrasion were noted in some shells. No signs of encrustation or bioerosion were observed.

Figure 11

574 4.3.3.1 Interpretation

575

576 Tempestites are formed by combined flows associated with unidirectional rip
577 currents and oscillatory flows, commonly generated by storms and hurricanes (Aigner,
578 1985; Seilacher and Aigner, 1991; Fürsich and Oschmann 1993; Clifton, 2006). Shell
579 concentration 3 is interpreted as distal tempestites deposited immediately above the
580 effective storm wave base (SWB).

581 At the bottom of the beds, most of the observed taphonomic characteristics (e.g.,
582 fragmented and dispersed bioclasts) are typically generated above the SWB (Brett 1995;
583 Simões and Torello, 2003; Bressan and Palma, 2010). However, their final preservation
584 is facilitated by the absence of background traction, suggesting a rise and change in the
585 SWB (e.g., Brett, 1990; Fürsich and Oschmann, 1993).

586 Massive to diffuse undulating cross stratification, interbedding with beds with
587 swaley stratification (facies Scs) point to a storm-dominated environment in the middle
588 shoreface (e. g. Myrow 2005). Shell concentrations range from loose to densely packed
589 toward to top of the beds, ending with larger shells forming pavement accumulations at
590 the upper boundary. This pattern of shell accumulation signals to reduction of net
591 sedimentation until total omission (see Kidwell, 1986 - Type I shell beds). In this sense,
592 the observed characteristics in shell concentration 3 are similar to those described for the
593 R-sediment model of Kidwell (1986).

594 According to Alván and Von Eynatten (2014), intermediate and distal tempestites
595 are intimately related to rapid waning of fine-grained particles below the fair-weather
596 wave base. The articulated closed shells preserved in the top of the biofabric (Figure 11
597 A) are interpreted as event concentrations (*sensu* Kidwell, 1998). Such shell

598 concentrations characterize biogenic concentrations formed by obruptions, preserving a
599 brief snapshot of living assemblage (Kidwell, 1998).

600

601

602

603

604

605

606

607

608

609

610

611

612

613

614

615

616

617

618

619

620

621

622

623 **5 Discussion**

624 5.1 Fossil concentration remarks

625 Manríquez et al. (2019) interpreted the base of the Man Aike Formation as a
626 shallow marine sequence under a transgressive system tract (TST). Their interpretation
627 agrees with the genetic processes suggested for fossil concentrations described in this
628 study. The fossiliferous lag concentration (Hsm), episodic concentration (Hgm_g), and the
629 storm-wave reworking deposits (Hgm_m - distal tempestites) are deposited by strictly
630 sedimentologic concentrations.

631 The fossiliferous lag concentrations are formed during sediment reworking within
632 a transgressive erosion, normally associated with the initial phase of TST in shoreface to
633 inner shelf environments (Kidwell, 1986;1989;1991; Bressan and Palma, 2010; Fick et
634 al., 2018; Fürsich and Oschmann 1993; Brett, 1995; Hendy et al., 2006; Parras and
635 Casadío, 2005; Yang 2007, Rigueti et al., 2020, Zecchin and Catuneanu, 2012).
636 Transgressive system tract typically preserve mixed and within-habitat transported
637 assemblages, reflecting high-energy environments with variable time-averaging and
638 species richness (Kidwell, 1998; Fürsich and Pandey, 2003; Zecchin and Catuneanu
639 2013; Earthal and Ritter, 2020). Thus, transgressive fossil concentrations are unlikely to
640 represent paleocommunities.

641 Taphonomic signatures such as polytypic infaunal-dominated assemblages,
642 within-habit time-averaged assemblages, disrupted biological patchiness upward within
643 beds, upward packing of bioclasts and pristine shells, as well as occurrence of glauconite,
644 are typical proxies for fossiliferous lags (Kidwell, 1989; Garcia-Ramos and Zuchin,
645 2019). The mixed features in lag concentrations of the Man Aike Formation (Hsm facies)
646 imply that they were exposed to numerous processes of erosion, reworking, winnowing
647 and deposition before the final burial. This would lead to skeletal concentrations with

648 high degree of temporal mixture. These deposits generated in upper to middle shoreface
649 are formed during shoreface erosion by waves and currents (Swift et al., 1986; Cattaneo
650 and Steel, 2003; Yang, 2007).

651 These fossiliferous lags can also accumulate in sites of persistent transport, and
652 episodic or continuous reworking processes in shoreface to inner shelf environments
653 (Kidwell et al., 1986; Kidwell, 1991; Bressan and Palma, 2010; Cattaneo and Steel, 2003;
654 Engelbrecht, 2000; Hendy et al., 2006; Parras and Casadío, 2005; Zecchin and Catuneanu,
655 2012). The absence of encrustation and bioeroded shells may also indicates high
656 sedimentation rates, related to high energy events like storms or strong currents (Kidwell,
657 1991; Hendy et al., 2006).

658 Better preservation is observed in the debris flow concentration of the Man Aike
659 Formation (Hgm_g facies), indicating brief permanence in the taphonomically active zone
660 (TAZ). The polytypic composition, mixing of taxa from different habitats and structures
661 diagnostic of storms activity suggest a sedimentological (hydraulic) build-up of skeletal
662 parts (Kidwell et al., 1986). In this case, the shell concentrations associated with debris
663 flow deposits was interpreted as episodic accumulations. Although, articulated bioclasts
664 infill with the same matrix as the rock, indicating close provenance for these bioclast.
665 The articulated shells, mixing of infaunal and epifaunal species (arborescent skeletons) is
666 an evidence of capture of infaunal skeletons by these erosive flows, followed by a rapid
667 burial of these parautochthonous assemblages (Brett and Baird, 1986; Kidwell, 1986;
668 Rigueti et al., 2020).

669 Sediment gravity flow-type facies characterize the overlaying mid/outer-shelf
670 deposits (Facies Hgm_g) of the Man Aike Formation, where associated with multiple
671 storm events, followed by post-tempestite deposition, producing hybrid sandstone layers
672 (Facies Hgmm). The strong cementation affecting the coarser tempestite layers is

673 consistent with reworking and amalgamation of storm events under low average
674 sedimentation rates. Upward the succession, oscillatory currents prevail, recorded in
675 swaley cross-stratified sandstones (Facies Scs), suggesting an increasing control of storm
676 activity (Swift et al., 1983; Greenwood and Sherman, 1986; Myrow, 2005; Dattilo et al.,
677 2012).

678 The storm-wave generated concentrations interpreted as distal tempestite. The
679 tempestite classification includes proximal shallow water settings (e.g., shoreface) to
680 deeper water (offshore transition to offshore) deposits (see Fürsich and Oschmann, 1993).
681 Proximal tempestites are composed of amalgamated thick deposits, commonly coarse-
682 grained and bioclastic supported. The bioclasts tend to show a good preservation (Einsele,
683 2000; Simões and Torello, 2003). Intermediate and distal tempestites are commonly few
684 cm to mm thick, with fine-grained amalgamated layers that commonly occur in the
685 offshore transition zone and may extend to the offshore shelf (Alvan and Von Eynatten,
686 2012). Shell beds in the distal tempestites tend to form thin pavements, well mixed and
687 with poorly preserved bioclasts (Aigner, 1985; Kidwell and Aigner, 1985; Seilacher and
688 Aigner, 1991; Simões and Torello, 2003; Dattilo et al., 2008; Schmidt-Neto et al., 2014).
689 However, in the Man Aike Formation the distal tempestite beds display a thicker layer.
690 This unusual characteristic is related to topographical features of this foreland basin. In
691 this sense, storms events can be able to rework deeper portions of the sea floor and
692 generate thicker beds in this type of basin.

693 The differences observed in the shell concentrations of the Eocene Man Aike
694 Formation are attributed to basin feature as well as the local environmental dynamic.
695 Eocene siliciclastic shallow water fossil concentrations of the Man Aike Formation are
696 interpreted as a deepening-trend cycle. Therefore, the basal deposits of the Man Aike
697 Formation are preserved above the ravinement surface that corresponds to begging of

698 TST (Figure 9). Toward to the top of the succession, fossil concentrations were deposited
699 in shoreface environment and middle to lower shoreface environment are observed,
700 respectively.

701 No significant taphonomic changes in the assemblage's were observed along the
702 studied interval. All fossil concentrations described here are infaunal-dominated with
703 large bivalves, along with subordinated multielements and gastropods. Therefore,
704 changes in patterns of taxa diversity, distribution and geometry of concentrations are
705 controlled by a complex interplay of large and small-scale environmental factors and
706 basin-scale processes (Hendy et al 2009; Leighton & Schneider, 2004).

707

708 5.2 Implications for Foreland Magallanes Basin

709

710 The coarse-grained lithologies, scarcity of bioturbation and the absence of fine
711 grained lithologies could be indicative of predominant bypass, reworking and winnowing
712 processes associated with high sedimentation rates and shelf construction processes
713 (Swift et al., 1987; Van de Meene et al., 1996). These could be indicative of a storm-
714 influenced reflective beach (Hamblin. & Walker, 1979; James and Mountjoy, 1983;
715 Myrow and Southard, 1991; Myrow, 2005; Naylor and Sinclair, 2008).

716 High energy and high relief coasts, near source area and slope settings, are
717 typically associated with foreland basin systems near wedge-top depositional zones
718 (Chiang and Chou, 2004; Conti et al., 2008; Pepe and Gallicchio, 2013). Such a setting
719 can explain the absence of fine-grained lithologies and the deposition of gravity flow-
720 type facies in the Man Aike Formation. Furthermore, thick distal tempestites can be
721 expected in this configuration, once slope steepening and width of the shelf are
722 significantly different from shallow open shelves. Additionally, short intertidal zones

723 would promote the alluvial discharges into the shoreface, producing shell concentrations
724 like those observed in the Fossil concentration 2 – Hgmg Facies (Figure 10) (McLaughlin
725 and Brett, 2007; Quaglio et al., 2014; Rivera et al., 2020). Therefore, studies reveal
726 complex interplay of sedimentation, tectonism, and base-level changes in Magallanes-
727 Austral Basin.

728

729 5.3 Paleoenvironmental evolution

730

731 Calcium content is relatively constant in the studied succession, without
732 displaying clear increases associate with the fossiliferous accumulations (shell beds). This
733 could be explained by the presence of Ca-rich minerals, such as plagioclases, and
734 carbonate cementation widespread along the succession (Figure 8 A, C, E, F, and I). This
735 pattern led us to infer that increased terr./Ca and Al/Ca ratios within the lowermost 10 m
736 of the studied succession were mainly driven by enhanced supply of terrigenous
737 sediments in the system. Therefore, decreasing-upward trends in the terr./Ca, Al/Ca and
738 Ti/Al suggest decreasing influx of land-derived material. These patterns may be related
739 with variations in riverine runoff intensity and/or relative sea-level rise (Bahr et al., 2008;
740 Spofforth et al., 2008; Itambi et al., 2009; Lebreiro et al., 2009; Nizou et al., 2010, 201
741 Beil et al., 2018). We favor that these trends were driven by a rise in relative sea level,
742 based on evidence from other proxy records, such as the Sr/Ca and the Ti/Al ratios.

743 Sr/Ca ratios also show a decreasing-upward trend. In Mediterranean Sea
744 sediments, Sr/Ca peaks in shallow marine settings, since high-Sr aragonite is
745 preferentially formed in these settings (Thomson et al., 2004; Rothwell et al., 2006; Grove
746 et al., 2010). The Ti/Al ratio is often used as a proxy for changes in the energy of
747 depositional processes, as well as riverine input intensity changes (Spofforth et al., 2008).

748 The decreasing-upward trend of Ti/Al in the studied section can be interpreted as a
749 decrease in the energy of depositional events upward in the section (Itambi et al., 2009;
750 Dickson et al., 2010). Chen et al. (2013) also showed that the Ti/Al molar ratio tends to
751 increase in locations closer the sediments sources. Therefore, we suggest that relatively
752 proximal (closer to the sediment sources) conditions were likely recorded by the
753 lowermost strata of the Man Aike Formation in the studied area. The decreasing upward
754 trend in $\log(\text{Zr/Rb})$ at the studied succession, indicate decreasing sediment grain sizes
755 (e.g. Spofforth et al., 2008; Beil et al., 2018), thus supporting the interpretation of a
756 deepening upward trend.

757 One open question, however, is whether this relative sea level change would be
758 related to global eustasy or to regional tectonic uplift. Since a foreland basin tends to
759 experience abrupt shift in sedimentation patterns, mainly when the deposition occurs near
760 to the orogenic wedge (see Dickinson, 1985), the conservative provenance of the
761 sediments assigned to the Man Aike Formation does not suggest the occurrence of any
762 major tectonic environmental events that could lead to a change in sedimentary sources
763 sources (Dickinson, 1985; Weltje and Evhatten, 2004). Conversely, global sea level
764 reconstruction during the Eocene point to transgressive episodes, coupled with warming
765 episodes, marked by a significant marine incursion over parts of southern South American
766 and the Antarctica Peninsula (Haq et al., 1987; Ivany et al., 2008; Malumián, 2002, Miller
767 and Gornitz, 2008; Huyghe et al., 2012; Payros et al., 2012; Westerhold et al., 2017;
768 Fossdick et al., 2020) during the middle Eocene. Furthermore, there is a correspondence
769 between high abundances of glauconite and the occurrence of warm climates during the
770 Paleogene (Zachos et al., 2001; Royer, 2006; Zachos et al., 2008; Benerjee et al., 2020).
771 Taken together, these observations make us favor a climatic forcing for the sea level rising
772 recorded by the Man Aike Formation

773 **6. Conclusion**

774

775 High resolution taphonomic, sedimentological, petrographic and geochemical
776 analyses of the lowermost Man Aike Formation enable to reconstruct depositional,
777 environmental and hydrodynamic settings of shallow marine middle Eocene strata
778 deposited at high latitudes in the Southern Hemisphere. Our data support previous
779 interpretations of a transgressive systems tract in shallow marine environment for the
780 lowermost part of the sequence, under influence of high energy process. The identified
781 deepening-upward trend may be linked with a larger accommodation space generated at
782 that time than the tectonic uplift, caused by the elevation of the Andes. Data suggest that
783 its primary cause was the middle Eocene high latitude warming, which was associated
784 with relative sea level rise. Sedimentary and taphonomic features indicate depositional
785 process related to mass flows in a steep shallow marine environment with coarse-grained
786 sediments, identified as concentrated granular flows. Also lag concentration formed in
787 proximal settings along the shoreface, displaying a wide lateral size and showing time
788 averaging, observed in taphonomic data. Tempestites also are identified formed in more
789 distal context by storms events, displaying thicker beds, here associated with the
790 paleogeography of the foreland basin under.

791

792

793

794

795

796

797

798 **6. Acknowledgements**

799

800 We thank National Counsel of Technological and Scientific Development (CNPq)
801 and (CAPES) for the research support and personal research grants (88887.372443/2019-
802 00). Acknowledgments also given to the Instituto Fossil (UNISINOS University) for the
803 laboratory facilities. The authors thank the Chilean Antarctic Institute (INACH Chile) for
804 the essential field assistance, collection, storage, and shipping of the samples, critical for
805 development to this research. This research was carried out within the terms of the
806 Agreement for Cooperation and Technical Assistance signed by the Antarctic Chilean
807 Institute (INACH Chile) which provided logistical support for this work with funding
808 provided by PROANTAR project (88887.314454/2019-00) and Anillo Project (ACT-
809 172099). We thank H.P. Kern for the valuable guidance and support. Especially, we
810 would also like to thank C. Trevisan, H. Ortiz, H. Mansilla and J.P. Pino for the good
811 reception and work support, and all that in some all contributed to improve this
812 manuscript. Photos credits for René Quinán. This paper contributes to the PROANTAR
813 Project (88887.314454/2019-00) – ‘‘Evolução climática do Paleoceno-Mioceno:
814 conexões entre o Oceano Austral e a Península Antártica’’.

815

816

817

818

819

820

821

822

823 **7. References**

- 824 Abbott, S. T. and Carte, R. M., (1997). Macrofossil associations from Mid-Pleistocene
825 cyclothem, Castlecliff Section, New Zealand: Implication for sequence stratigraphy:
826 *Palaios*, v. 12, p. 188–210.
- 827 Alarcón-Muñoz, J., Soto-Acuña, S., Manríquez, L. M., Fernández, R. A., Bajor, D.,
828 Guevara, J. P., Suazo, F., Leppe, M., and Vargas, A. O. (2020). Freshwater turtles
829 (Testudines: Pleurodira) in the Upper Cretaceous of Chilean Patagonia. *Journal of South*
830 *American Earth Sciences*, 102652.
- 831 Alván, A., and Von Eynatten, H., (2014). Sedimentary facies and stratigraphic
832 architecture in coarse-grained deltas: Anatomy of the Cenozoic Camaná Formation,
833 southern Peru (16°25'S to 17°15'S). *Journal of South American Earth Sciences*, 54, 82–
834 108. <https://doi.org/10.1016/j.jsames.2014.04.008>
- 835 Amorim, K. B., Afonso, J. W. L., Leme, J. de M., Diniz, C. Q. C., Rivera, L. C. M.,
836 Gómez-Gutiérrez, J. C., Boggiani, P. C., and Trindade, R. I. F., (2020). Sedimentary
837 facies, fossil distribution and depositional setting of the late Ediacaran Tamengo
838 Formation (Brazil). *Sedimentology*, 67(7), 3422–3450.
839 <https://doi.org/10.1111/sed.12749>
- 840 Anderson, L., and McBride, R., (1996). Taphonomic and Paleoenvironmental Evidence
841 of Holocene Shell-Bed Genesis and History on the Northeastern Gulf of Mexico Shelf.
842 *Palaios*, 11(6). 532-549. doi:10.2307/3515189
- 843 Aigner T, Reineck H. E., (1982) Proximal trends in modern storm sands from the
844 Helgoland Bight (North Sea) and their implications for basin analysis. *Senckenb Marit*
845 14: 183–215.
- 846 Aigner, T. (1985). *Storm Depositional Systems: Dynamic Stratigraphy in Modern and*
847 *Ancient Shallow-Marine Sequences*. Springer Berlin Heidelberg, p. 174.

848 Allen, J. R. L. (1963). The Classification of Cross-Stratified Units. With Notes on Their
849 Origin. *Sedimentology*, 2: 93-114. <https://doi.org/10.1111/j.1365-3091.1963.tb01204.x>

850 Alexander, J., Bridge, J. S., Cheel, R. J., and Leclair, S. F. (2001). Bedforms and
851 associated sedimentary structures formed under supercritical water flows over aggrading
852 sand beds. *Sedimentology*, 48(1), 133–152.

853 Amorim, K. B., Afonso, J. W. L., Leme, J. de M., Diniz, C. Q. C., Rivera, L. C. M.,
854 Gómez-Gutiérrez, J. C., Boggiani, P. C., and Trindade, R. I. F., (2020). Sedimentary
855 facies, fossil distribution and depositional setting of the late Ediacaran Tamengo
856 Formation (Brazil). *Sedimentology*. 67(7), 3422–3450.
857 <https://doi.org/10.1111/sed.12749>

858 Aragón, E., Pinotti, L., Fernando, D., Castro, A., Rabbia, O., Coniglio, J., and Aguilera,
859 Y. E., (2013). The Farallon-Aluk ridge collision with South America: Implications for the
860 geochemical changes of slab window magmas from fore-to back-arc. *Geoscience
861 Frontiers*, 4(4), 377-388.

862 Arnott, R. W., and Southard, J. B., (1990). Exploratory flow-duct experiments on
863 combined-flow bed configurations, and some implications for interpreting storm-event
864 stratification. *Journal of Sedimentary Research*, 60(2), 211-219.

865 Bahr, A., Lamy, F., Arz H. W., Major, C., Kwiecien, O., and Wefer, G., (2008). Abrupt
866 changes of temperature and water chemistry in the late Pleistocene and early Holocene
867 Black Sea. *Geochem Geophys Geosyst* 9: Q01004. doi:1029/2007GC001683

868 Banerjee, S., Choudhury, T.R., Saraswati, P.K. Khanolkar S., (2020). The formation of
869 authigenic deposits during Paleogene warm climatic intervals: a review. *J.
870 Palaeogeogr.*9,27 <https://doi.org/10.1186/s42501-020-00076-8>

871 Barrio, C. A. (1990b). Late Cretaceous - Early Tertiary sedimentation in a semi-arid
872 foreland basin (Neuquén Basin, western Argentina). *Sedimentary Geology* 66: 255-275.

873 Beckvar, N., and Kidwell, S. M. (1988). Hiatal shell concentrations, sequence analysis,
874 and sealevel history of a Pleistocene coastal alluvial fan, Punta Chueca, Sonora. *Lethaia*,
875 21(3), 257-270.

876 Beil, S., Kuhnt, W., Holbourn, A.E., Aquit, M., Flögel, S., Chellai, E.H., and Jabour, H.,
877 (2018). New insights into Cenomanian paleoceanography and climate evolution from the
878 Tarfaya Basin, southern Morocco. *Cretac. Res.* 84, 451–473. [https://doi.org/10.](https://doi.org/10.1016/j.cretres.2017.11.006)
879 [1016/j.cretres.2017.11.006](https://doi.org/10.1016/j.cretres.2017.11.006)

880 Biddle, K.T., Uliana, M.A., Mitchum, R.M. Jr, Fitzgerald, M.G., and Wright, R.C.,
881 (1986). The stratigraphic and structural evolution of the Central and Eastern Magallanes
882 Basin, southern South America. In: Allen, P.A., Homewood, P. (Eds.), *Foreland Basins*,
883 International Association of Sedimentologists, Special Publication, vol. 8. Blackwell
884 Science Publication, Oxford, pp. 41–61.

885 Boyer, D. L., Bottjer, D. J., and Droser, M. L., (2004). Ecological signature of Lower
886 Triassic shell beds of the western United States. *Palaios*, 19(4), 372-380.

887 Brett, C. E., Baird, G. C., (1986). Comparative taphonomy; a key to paleoenvironmental
888 interpretation based on fossil preservation. *Palaios*, 1(3), 207-227.

889 Brett, C. E., (1990). Destructive taphonomic processes and skeletal durability. In: D.E.G.
890 Briggs & C. Peter (eds.) *Palaeobiology a synthesis*, Blackwell Science Ltd, p. 223-226.

891 Brett, C. E. (1995). Sequence Stratigraphy, Biostratigraphy, and Taphonomy in Shallow
892 Marine Environments. In *Palaios* (Vol. 10, Issue 6, p. 597).
893 <https://doi.org/10.2307/3515097>.

894 Brett, Carlton E. Hendy, Austin J.W. Bartholomew, Alex J. Bonelli, James R.
895 Mclaughlin; and Patrick I., (2007). Response of Shallow Marine Biotas to Sea-Level
896 Fluctuations: A Review of Faunal Replacement and the Process of habitat tracking.
897 *Palaios*; 22 (3): 228–244. <https://doi.org/10.2110/Palo.2005.P05-028r>

898 Bressan, G. S., and Palma, R. M., (2010). Taphonomic analysis of fossil concentrations
899 from La Manga Formation (Oxfordian), Neuquén Basin, Mendoza Province, Argentina.
900 *Journal of Iberian Geology*, 36(1), 55–71. <https://doi.org/10.5209/JIGE.33868>

901 Bromley, R. G. (1996). *Trace Fossils: Biology, Taphonomy and Applications*. 2^o edition.
902 Springer-Science+Business Media, B.V.

903 Camacho, H.H., Chiesa, J.O., Parma, S.G., and del Río, C., (2000). Invertebrados marinos
904 eocenos de los cerros Palique y Castillo, sudoeste de la provincia de Santa Cruz,
905 Argentina. *Ameghiniana*, 37, 59-72.

906 Casadío, S. A., Griffin, M., Marensi, S. A., Net, L. I., Parras, A. M., Rodriguez Raising,
907 M. E., and Santillana, S. (2009). Paleontology and sedimentology of Middle Eocene rocks
908 in Lago Argentino area, Santa Cruz Province, Argentina. *Ameghiniana* 46:27-48.

909 Cattaneo, A., and Steel, R. J. (2003). Transgressive deposits: A review of their variability.
910 *Earth-Science Reviews*, 62(3–4), 187–228. [https://doi.org/10.1016/S0012-](https://doi.org/10.1016/S0012-8252(02)00134-4)
911 [8252\(02\)00134-4](https://doi.org/10.1016/S0012-8252(02)00134-4)

912 Conti, S., Fontana, D., and Lucente, C. C. (2008). Sedimentary filling of a wedge-top
913 basin and relationship with the foredeep (Middle Miocene Marnoso-arenacea Formation,
914 (northern Apennines). *Facies*, 54(4), 479–498. [https://doi.org/10.1007/s10347-008-0153-](https://doi.org/10.1007/s10347-008-0153-5)
915 [5](https://doi.org/10.1007/s10347-008-0153-5)

916 Cuitiño, J. I., Varela, A. N., Ghiglione, M. C., Richiano, S., and Poiré, D. G. (2019). The
917 Austral-Magallanes Basin (southern Patagonia): A synthesis of its stratigraphy and
918 evolution. *Latin American Journal of Sedimentology and Basin Analysis*, 26(2), 155–
919 166.

920 Chen, H. F., Yeh, P. Y., Song, S. R., Hsu, S. C., Yang, T. N., Wang, Y., Chi, Z., Lee, T.
921 Q., Chen, M. Te, Cheng, C. L., Zou, J., and Chang, Y. P., (2013). The Ti/Al molar ratio
922 as a new proxy for tracing sediment transportation processes and its application in aeolian

923 events and sea level change in East Asia. *Journal of Asian Earth Sciences*, 73, 31–38.
924 <https://doi.org/10.1016/j.jseaes.2013.04.017>

925 Chiang, C., Yu, H., and Chou, Y., (2004). Characteristics of the wedge-top depozone of
926 the southern Taiwan foreland basin system. 65–78. <https://doi.org/10.1111/j.1365->
927 [2117.2003.00222.x](https://doi.org/10.1111/j.1365-2117.2003.00222.x)

928 Clifton, H. E., (2003). Supply, segregation, successions, and significance of shallow
929 marine conglomeratic deposits. *Bulletin of Canadian Petroleum Geology*, 51(4), 370–
930 388.

931 Clifton, H. E., (2006). A re-examination of facies models for clastic shorelines. In:
932 Posamentier, H.W., Walker, R.G. (Eds.), *Facies Models Revisited*. Society for
933 *Sedimentary Geology Special Publication*. Vol. 84, 293-337.

934 Daniels, B. G., Auchter, N. C., Hubbard, S. M., Romans, B. W., Matthews, W. A., and
935 Stright, L. (2018). Timing of deep-water slope evolution constrained by large-n detrital
936 and volcanic ash zircon geochronology, Cretaceous Magallanes Basin, Chile. *GSA*
937 *Bulletin*, 130(3-4), 438-454.

938 Dasgupta, P., (2003). Sediment gravity flow - the conceptual problems. *Earth Sci. Rev.*
939 62, 265–281.

940 Dasgupta, P. and Priyanka Manna. (2011): “Geometrical mechanism of inverse grading
941 in grain-flow deposits: An experimental revelation.” *Earth-Science Reviews* 104, 186-
942 198.

943 Davies, P. J., Symonds, P. A., Feary, D. A., and Pigram, C. J., (1989). The evolution of
944 the carbonate platforms of northeast Australia. – In: Crevello, P. G., Wilson, J. J., Sarg,
945 J. F. and Read, J. F. (eds.): *Carbonate Platform and Basin Development*. Soc. Econ.
946 *Petrol. Min. (Society for Sedimentary Geology) Spec. Publ.* 44, 233–257.

947 Dattilo, B. F., Brett, C. E., Tsujita, C. J., and Fairhurst, R. (2008). Sediment supply versus
948 storm winnowing in the development of muddy and shelly interbeds from the Upper
949 Ordovician of the Cincinnati region, USA. *Canadian Journal of Earth Sciences*, 45(2),
950 243–265. <https://doi.org/10.1139/E07-060>

951 Dattilo, B. F., Brett, C. E., and T. J., (2012). Tempestites in a teapot? Condensation-
952 generated shell beds in the Upper Ordovician, Cincinnati Arch, U.S.A. *Palaeogeography,*
953 *Palaeoclimatology, Palaeoecology*, 367–368:44–62.

954 Decelles, P. G., and Giles, K. A., (1996). Foreland basin systems. 105–123.

955 De Souza, E. G., Scherer, C. M. S., dos Reis, A. D., Bállico, M. B., Ferronato, J. P. F.,
956 Boffill, L. M., Kifumbi, C., (2019). Sequence stratigraphy of the mixed wave-tidal-
957 dominated Mesoproterozoic sedimentary succession in Chapada Diamantina Basin,
958 Espinhaço supergroup— Ne/Brazil. *Precambrian Research*, 327, 103–120.
959 <https://doi.org/10.1016/j.precamres.2019.03.007>

960 Dickinson, W. R., (1985) Interpreting provenance relations from detrital modes of
961 sandstones. In: Zuffa, G.G. (Ed.), *Provenance of Arenites*. D. Reidel Publishing
962 Company, 1985, 333-363

963 Dickson, A. J., Leng, M. J., Maslin M. A., Röhl U., (2010). Oceanic, atmospheric and
964 ice-sheet forcing of Southeast Atlantic Ocean productivity and South African monsoon
965 intensity during MIS-12 to 10. *Quat Sci Rev* 29:3936–3947. doi:
966 10.1016/j.quascirev.2010.09.014

967 Duke, W. L., (1985). Hummocky cross-stratification, tropical hurricanes, and intense
968 winter storms. *Sedimentology*, 32(2):167-194.

969 Duke, W. L., (1987). Hummocky cross-stratification, tropical hurricanes, and intense
970 winter storms—Reply: *Sedimentology*, v. 34, p. 344–359.

971 Duke, W. L., Arnott R.W.C., Cheel R. J., (1991). Shelf sandstones and hummocky cross-
972 stratification: new insights on a stormy debate. *Geology*, 19(6):625-628.

973 Dumas, S., Arnott R. W. C., (2006). Origin of hummocky and swaley crossstratification
974 - the controlling influence of unidirectional current strength and aggradation rate.
975 *Geology*, 34(12):1073-1076. <https://doi.org/10.1130/G22930A.1>

976 Dypvik, H., Harris N.B. (2001). Geochemical facies analysis of fine-grained siliciclastics
977 using Th/U,Zr/Rb and (Zr + Rb)/Sr ratios. *Chem Geol* 181:131–146

978 Erthal, F. and do Nascimento Ritter M. (2020). Taphonomy of recent bioclastic deposits
979 from the Southern Brazil shelf: Stratigraphic Potential. In: Martínez S., Rojas A., Cabrera
980 F. (eds) *Actualistic Taphonomy in South America. Topics in Geobiology*, vol 48.
981 Springer, Cham. https://doi.org/10.1007/978-3-030-20625-3_1

982 Eagles, G., Jokat, W. (2014). Tectonic reconstructions for paleobathymetry in Drake
983 Passage. *Tectonophysics*, 611, 28-50.

984 Fick, C., Toldo Jr, E. E., and Puhl, E. (2018). Shell concentration dynamics driven by
985 wave motion in flume experiments: Insights for coquina facies from lake-margin settings.
986 *Sedimentary Geology* 374, 98-114.

987 Fildani, A., Cope, T.D., Graham, S.A., Wooden, J.L. (2003). Initiation of the Magallanes
988 Foreland Basin: Timing of the Southernmost Patagonian Andes Orogeny Revised by
989 Detrital Zircon Provenance Analysis. *Geology* 3, 1081-1084.

990 Fildani, A., Romans, B. W., Fosdick, J. C., Crane, W. H., and Hubbard, S. M., (2008).
991 Orogenesis of the Patagonian Andes as reflected by basin evolution in southernmost
992 South America. *Arizona Geological Society Digest*, 22, 259-268.

993 Fosdick, J., Romans B., Fildani A., Bernhardt A., Calderón M., and Graham S.A., (2011).
994 Kinematic Evolution of The Patagonian Retroarc Fold-Thrust Belt and Magallanes

995 Foreland Basin, Chile and Argentina, 51°30's. Geological Society of America Bulletin,
996 123 (9/10):1679–1698.

997 Fosdick, J. C., Bostelmann, J. E., Leonard, J., Ugalde, R., Oyarzún, J. L., Griffin, M., (2015a). Ti
998 mingandratesofforelandsedimentation:newdetritalzirconU/PbgeochronologyoftheCerro
999 Dorotea. In: Río Turbio, and Río Guillermo Formations, Magallanes Basin. XIV Congreso Geo
1000 lógico Chileno, La Serena, Chile, Abstracts with Program, pp. 763-766.

1001 Fosdick, J. C., Grove, M., Graham, S. A., Hourigan, J. K., Loveras, O., Romans, B. W., (2015b).
1002 Detrital thermochronologic record of burial heating and sediment re cycling in the
1003 Magallanes foreland basin, Patagonian Andes. *Basin Res.* 27, 546–572.

1004 Fosdick, J. C., VanderLeest, R. A., Bostelmann, J. E., Leonard, J. S., Ugalde, R., Oyarzún,
1005 J. L., and Griffin, M., (2020). Revised Timing of Cenozoic Atlantic Incursions and
1006 Changing Hinterland Sediment Sources during Southern Patagonian Orogenesis.
1007 *Lithosphere*, 2020(1), 1–18. <https://doi.org/10.2113/2020/8883099>

1008 Futterer, E., (1978). Studien über die Ein-regelung, Anlagerung und Einbettung biogener
1009 Hartteile im Stromungskanal: Neues Jahrbuch für Geologie und Paläontologie
1010 Abhandlungen, v. 156, p. 87- 131.

1011 Fürsich, F. T., and Oschmann, W. (1993). Shell Beds as Tools in Basin Analysis: The
1012 Jurassic of Kachchh, Western India. *Journal of The Geological Society*, 150(1), 169-185.

1013 Fürsich, F. T. (1995). Approaches to paleoenvironmental reconstructions. *Geobios*, 28,
1014 183-195.

1015 Fürsich F, T, Pandey D, K., (2003). Sequence stratigraphic significance of sedimentary
1016 cycles and shell concentrations in the Upper Jurassic-Lower Cretaceous of Kachchh,
1017 western India. *Paleogeogr Paleoclimatol Paleoecol* 193:285–309.

1018 García-Ramos, D. A., and Zuschin, M., (2019). High-frequency cycles of brachiopod
1019 shell beds on subaqueous delta-scale clinoforms (early Pliocene, south-east Spain).
1020 *Sedimentology*, 66(5), 1486–1530. <https://doi.org/10.1111/sed.12541>

1021 George, S. W., Davis, S. N., Fernández, R. A., Manríquez, L. M., Leppe, M. A., Horton,
1022 B. K., and Clarke, J. A. (2020). Chronology of deposition and unconformity development
1023 across the Cretaceous–Paleogene boundary, Magallanes-Austral Basin, Patagonian
1024 Andes. *Journal of South American Earth Sciences*, 102237.

1025 Goin, F., Martinelli, A., Soto-Acuña, S., Vieytes, E., Manríquez, L., Fernández, R., Pino,
1026 J.P., Trevisan, C., Kaluza, J., Reguero, M., Leppe, M., Ortiz, H., Rubilar-Rogers, D.,
1027 Vargas. A. (2020). First Mesozoic Mammal from Chile: The Southernmost record of Late
1028 Cretaceous Gondwanatherian. *Boletín del Museo de Historia Natural, Chile*, 69 (1): 5-31

1029 Gutiérrez, N.M., Le Roux, J.P., Vásquez, A., Carreño, C., Pedroza, V., Araos, J.,
1030 Oyarzún, J.L., Pino, J.P., Rivera, H.A., Hinojosa, L.F., (2017). Tectonic Events Reflected
1031 by Palaeocurrents, Zircon Geochronology, and Palaeobotany in the Sierra Baguales of
1032 Chilean Patagonia. *Tectonophysics* 695, 76-99.

1033 Grove, C.A., Nagtegaal R., Zinke J., Scheufen T., Koster B., Kasper S., McCulloch M.T.,
1034 Van den Bergh G., Brummer G.J.A. (2010). River runoff reconstructions from novel
1035 spectral luminescence scanning of massive coral skeletons. *Coral Reefs* 29:579–591.
1036 [doi:10.1007/s00338-010-0629-y](https://doi.org/10.1007/s00338-010-0629-y)

1037 Hart, B. S., & Plint, A. G. (1989). Gravelly shoreface deposits: a comparison of modern
1038 and ancient facies sequences. *Sedimentology*, 36(4), 551–557.
1039 <https://doi.org/10.1111/j.1365-3091.1989.tb02085.x>

1040 Haq, B. U., Hardenbol, J., and Vail, P. R., (1987). Chronology of fluctuating sea levels
1041 since the Triassic (250 million years ago to present). *Science*, 235, 1156–1167.

1042 Hamblin, A. P, and G. Walker. R. G., (1979). Storm-dominated shallow marine deposits:
1043 the Fernie–Kootenay (Jurassic) transition, southern Rocky Mountains. *Canadian Journal*
1044 *of Earth Sciences*. 16(9): 1673-1690.

1045 Harms, J. C.; Southard, J. B.; and Walker, R. G., (1982). Structures and sequences in
1046 clastic rocks: SEPM Short Course Notes 9, 249 p.

1047 Harambour, S.M.; Soffía, J.M. 1988. Transición desde margen pasivo a cuenca de
1048 antepaís: modelo de evolución para el extremo norte de Última Esperanza, Magallanes,
1049 Chile. In *Congreso Geológico Chileno*, No. 5, Actas, Vol. 1, p. 385-402. Santiago.

1050 Hendy, A.J.,Kamp, P.J. and Vonk, A.J. (2006). Cool-watershell bed taphofacies from
1051 Miocene-Pliocene shelfsequences in New Zealand utility of taphofacies in sequence
1052 stratigraphic analysis. In: *Cool-Water Carbonates: Depositional Systems and*
1053 *Palaeoenvironmental Controls* (Eds H.M. Pedley and G.Carannante), Geological Society,
1054 London, *SpecialPublications*, 255, 283–305.

1055 Hendy, A. J., Kamp, P. J., & Vonk, A. J., (2009). Late Miocene turnover of molluscan
1056 faunas, New Zealand: Taxonomic and ecological reassessment of diversity changes at
1057 multiple spatial and temporal scales. *Palaeogeography, Palaeoclimatology,*
1058 *Palaeoecology*, 280(3-4), 275-290. doi:10.1016/j.palaeo.2009.06.010

1059 Holland, S.M., (2000). The quality of the fossil record: a sequence stratigraphic
1060 perspective. In: Erwin, D.H., Wing, S.L. (Eds.), *Deep time: paleobiology’s perspective*.
1061 The Paleontological Society, Lawrence, KS, pp. 148– 168.

1062 Holland, S.M., (2001). Sequence stratigraphy and fossils. In: Briggs, D.E.G., Crowther,
1063 P.R. (Eds.), *Palaeobiology*, vol. II. Blackwell Science, Oxford, pp. 548– 553.

1064 Huyghe, D., Merle, D. Lartaud, F. Cheype, E. and Laurent E. (2012). Middle Lutetian
1065 climate in the Paris Basin: implications for a marine hotspot of paleobiodiversity. *Facies*
1066 58, 587–604 (2012). <https://doi.org/10.1007/s10347-012-0307-3>

1067 Holz, M., and Simoes, M. G. (2005). Applied Stratigraphy. In Applied Stratigraphy (Issue
1068 November (2016). <https://doi.org/10.1007/1-4020-2763-x>

1069 Horodyski, R. S., Brett, C. E., Sedorko, D., Bosetti, E. P., Scheffler, S. M., Ghilardi, R.
1070 P., and Iannuzzi, R. (2019). Storm-related taphofacies and paleoenvironments of
1071 Malvinokaffric assemblages from the Lower/Middle Devonian in southwestern
1072 Gondwana. *Palaeogeography, Palaeoclimatology, Palaeoecology*, 514(October), 706–
1073 722. <https://doi.org/10.1016/j.palaeo.2018.10.001>

1074 Itambi, A.C., Von Dobeneck, T. Mulitza, S., Bickert, T., and Heslop, D. (2009).
1075 Millennial-scale northwest African droughts related to Heinrich events and Dansgaard-
1076 Oeschger cycles: evidence in marinesediments from offshore Senegal. *Paleoceanography*
1077 24:PA1205. doi:10.1029/2007PA001570.

1078 Ivany, L. Lohmann, K. & Hasiuk, Franciszek & Blake, Daniel and Glass, Alexander and
1079 Aronson, Richard & Moody, Ryan., (2008). Eocene climate record of a high southern
1080 latitude continental shelf: Seymour Island, Antarctica. *Geological Society of America*
1081 *Bulletin - Geol Soc Amer Bull.* 120. 10.1130/B26269.1.

1082 Johnson H. D., and Baldwin C.T., (1996). Shallow clastic seas. In: Reading H.G. (ed).
1083 *Sedimentary environments: Processes, Fácies and Stratigraphy.* Oxford, Blackwell
1084 Science, p. 232-280

1085 Kern, H. P., Lavina, E. L. C., Paim, P. S. G., Leanza, H. A. (2019). Stratigraphic evolution
1086 of the nearshore to fluvial plain of the Upper Cuyo Group, Neuquén, Argentina.
1087 *Sedimentology*, 66(7), 2686–2720.

1088 Kennedy, M., (2015). Chapter 2 - Petrophysical Properties, Editor(s): Martin Kennedy,
1089 *Developments in Petroleum Science*, Elsevier, Volume 62, Pages 21-72, ISSN 0376-
1090 7361, ISBN 9780444632708.

1091 Kidwell, S. M., Aigner, T., (1985). Sedimentary Dynamics of Complex Shell Beds;
1092 Implications for Ecologic and Evolutionary Patterns, in: Seilacher, A., Friedman, G.M.
1093 (Eds.), Sedimentary and evolutionary cycles. Tubingen, Federal Republic of Germany.
1094 Kidwell, S. M. (1986). Models for fossil concentrations: paleobiologic implications.
1095 *Paleobiology*, 6-24.

1096 Kidwell, S. M., Fürsich, F.T., Aigner, T. (1986). Conceptual Framework for the Analysis
1097 and Classification of Fossil Concentrations. *Palaios* 1, 228–238.

1098 Kidwell, S. M. (1989). Stratigraphic condensation of marine transgressive records: origin
1099 of major shell deposits in the Miocene of Maryland. *J. Geol.* 97:1–24.

1100 Kidwell S. M. (1998). Time-averaging in the marine fossil record: overview of strategies
1101 and uncertainties. [Détermination de la durée d'accumulation dans le registre fossile
1102 marin: revue des stratégies et des incertitudes]. *GEOBIOS*, 30, 7: 977-995. Villeurbanne,
1103 le 31.03.1998.

1104 Kidwell, S. M., (1991). The stratigraphy of shell concentrations. In: Allison PA, Briggs
1105 DEG (eds) *Taphonomy. Releasing the Data Locked in the Fossil Record*. Plenum Press,
1106 New York: 211 -290.

1107 Kidwell, S. M. and Holland, S. M. (1991). Field Description of Coarse Bioclastic Fabric.
1108 *Palaios*, V. 6, P. 426–434.

1109 Kraemer, P. E., Ploszkiewicz, J. V., and Ramos, V. A. (2002). Estructura de la Cordillera
1110 Patagónica Austral entre los 46 y 52 S. In *Geología y Recursos Naturales de la provincia*
1111 *de Santa Cruz. Relatorio del 15 Congreso Geológico Argentino*, El Calafate, Santa Cruz,
1112 Asociación Geológica Argentina (pp. 353-364).

1113 Legarreta, L., and Gulisano, C. A. (1989). Análisis estratigáfico secuencial de la Cuenca
1114 Neuquina (Triásico superior-Terciario inferior). *Serie Correlación Geológica* 6, 419–442.
1115 S.M. de Tucumán.

1116 Le Roux, J. P., Puratich, J., Mourgues, A., Oyarzún, J.L., Otero, R.A., Torres, T., Hervé,
1117 F., (2010). Estuary deposits in the Río Baguales Formation (Chattian-Aquitanean),
1118 Magallanes Province, Chile. *Andean Geol.* 37, 329–344.

1119 Leckie, D. A., and Walker, R. G., (1982). Storm-and tide-dominated shorelines in
1120 cretaceous moose bar-lower gates interval–outcrop equivalents of deep basin gas trap in
1121 western Canada. *AAPG Bull.* 66, 138–157

1122 Lebreiro S. M, Voelker AHL, Vizcaino A, Abrantes FG, Alt-Epping U, Jung S, Thouveny
1123 N, Gràcia E. (2009). Sediment instability on the Portuguese continental margin under
1124 abrupt glacial climate changes (last 60 kyr). *Quat Sci Rev* 28:3211–3223. doi:
1125 10.1016/j.quascirev.2009.08.007

1126 Lima, C. C. U., and Boas, G. D. S. V., (1994). Mecanismos de transporte e deposição dos
1127 conglomerados da Formação Marizal (Cretáceo Inferior) Na Bacia Do Recôncavo, Bahia,
1128 Brasil. *Revista Brasileira de Geociências*, 24(4), 240–246. [https://doi.org/10.25249/0375-](https://doi.org/10.25249/0375-7536.1994240246)
1129 [7536.1994240246](https://doi.org/10.25249/0375-7536.1994240246)

1130 Livermore, R., Nankivell, A., Eagles, G., and Morris, P. (2005). Paleogene opening of
1131 Drake passage. *Earth and Planetary Science Letters*, 236(1-2), 459-470.

1132 Lowe, D. R., (1979). Sediment gravity flows: their classifications and some problems of
1133 application to natural flows and deposits. In: Doyle, L.J., Pilkey, O.H. (Eds.), *Geology of*
1134 *Continental Slopes*. Spec. Publ. - Soc. Econ. Paleontol. Mineral., vol. 27, pp. 75 – 82.

1135 Lowe, D. R. (1982). Sediment gravity flows: II. Depositional models with special
1136 reference to the deposits of high-density turbidity currents. *J. Sediment. Petrol.* 52, 279 –
1137 297.

1138 Maahs, R., Küchle, J., dos Santos Scherer, C. M., & dos Santos Alvarenga, R. (2019).
1139 Sequence stratigraphy of fluvial to shallow-marine deposits: The case of the early

1140 Permian Rio Bonito Formation, Paraná Basin, southernmost Brazil. *Brazilian Journal of*
1141 *Geology*, 49(4). <https://doi.org/10.1590/2317-4889201920190059>

1142 MacEachern, J. A., and Pemberton, S.G. (1992). Ichnological aspects of Cretaceous
1143 shoreface successions and shoreface variability in the Western Interior Seaway of North
1144 America. In: Pemberton, S.G.(Ed.), *Applications of Ichnology to Petroleum Exploration*.
1145 *SEPM Core Workshop Notes* 17, pp. 57–84.

1146 MacEachern, J.A., Zaitlin, B.A., Pemberton, S.G., (1999b). A sharp-based sandstone
1147 succession of the Viking Formation, Joffre Field, Alberta, Canada: criteria for recognition
1148 of transgressively incised shoreface complexes. *J. Sediment. Res.* 69, 876–892.

1149 MacEachern, J. A., and Gingras, M. K., (2007). Recognition of brackishwater trace fossil
1150 assemblages in the Cretaceous Western Interior Seaway of Alberta, in Bromley, R.,
1151 Buatois, L.A., Genise, J., Mángano, M.G., and Melchor, R., eds., *Sediment–Organism*
1152 *Interactions: A Multifaceted Ichnology*: SEPM, Special Publication 88, p. 149–193.

1153 Malkowski, M. A., Schwartz, T. M., Sharman, G. R., Sickmann, Z. T., and Graham, S.
1154 A., (2017). Stratigraphic and Provenance Variations in the Early Evolution of the
1155 Magallanes-Austral Foreland Basin: Implications for the Role of Longitudinal Versus
1156 Transverse Sediment Dispersal during Arc-Continent Collision. *Bulletin*, 129(3-4), 349-
1157 371.

1158 Malumián, N., and Caramés, A., (1997). Upper Campanian-Paleogene from the Río
1159 Turbio coal measures in southern Argentina: Micropaleontology and the
1160 Paleocene/Eocene boundary. *Journal of South American Earth Sciences*, 10(2), 189–201.
1161 [https://doi.org/10.1016/s0895-9811\(97\)00015-1](https://doi.org/10.1016/s0895-9811(97)00015-1)

1162 Malumián, N., Panza, J. L. A., and Parisi, C. (2000). *Hoja Geológica 5172-III Yacimiento*
1163 *Río Turbio*.

1164 Malumián, N., (2002). El Terciario marino. Sus relaciones con el eustatismo. En M.J.
1165 Haller (Ed.), *Geología y Recursos naturales Proserpio*, C.A., 1980. Descripción
1166 Geológica de la Hoja 58 a-b lago Viedma, provincia de Santa Cruz. Servicio Geológico
1167 Nacional, Inédito.

1168 Malumián, N. and Nández, C., (2011). The Late Cretaceous–Cenozoic transgressions in
1169 Patagonia and the Fuegian Andes: foraminifera, palaeoecology, and palaeogeography,
1170 *Biological Journal of the Linnean Society*, Volume 103, Issue 2, June, Pages 269–288.

1171 Marensi, S. A., Casadío, S., and Santillana, S., (2002). La Formación Man Aike al sur
1172 de el Calafate (Provincia De Santa Cruz) y su relación con la discordancia del Eoceno
1173 Medio en la Cuenca Austral. *Revista de la Asociación Geológica Argentina* 57 (3), 341-
1174 344.

1175 Marensi, S. A., Casadío, S., and Santillana, S. N., (2003). Estratigrafía y Sedimentología
1176 de las Unidades del Cretácico Superior-Paleógeno Aflorantes en la Margen Sureste Del
1177 Lago Viedma, Provincia De Santa Cruz, Argentina. *Revista De La Asociación Geológica*
1178 *Argentina* 58(3), 403-416.

1179 Manríquez, L. M., Lavina, E. L., Fernández, R. A., Trevisan, C., and Leppe, M. A. (2019).
1180 Campanian-Maastrichtian and Eocene Stratigraphic Architecture, Facies Analysis, and
1181 Paleoenvironmental Evolution of the Northern Magallanes Basin (Chilean Patagonia).
1182 *Journal of South American Earth Sciences*, 93, 102-118.

1183 Manville, V. and White, J. (2003). Incipient granular mass flows at the base of sediment-
1184 laden floods, and the roles of flow competence and flow capacity in the deposition of
1185 stratified bouldery sands. *Sedimentary Geology*. 155. 157-173. 10.1016/S0037-
1186 0738(02)00294-4

1187 Martinelli, A., Soto-Acuña, S., Goin, F.J., Kaluza, J., BostelmanN, J.E., Fonseca, P.H.M.,
1188 Reguero, M.A., Leppe, M., and Vargas, A.O. (2021). New cladotherian mammal from

1189 southern Chile and the evolution of mesungulatid meridiolestidans at the dusk of the
1190 Mesozoic era. *Scientific Reports*, <https://doi.org/10.1038/s41598-021-87245-4>.

1191 Mella, P. (2001). Control tectónico en la evolución de la Cuenca de antepaís de
1192 Magallanes, XII Región, Chile. *Memória para optar al título de Geólogo*. Universidad De
1193 Concepción, Departamento De Ciências De La Tierra (Inédito), 149 Pp.

1194 Miall, A. D. (1996): *The Geology of Fluvial Deposits, Sedimentary Facies, Basin*
1195 *Analysis and Petroleum Geology*. – Springer-Verlag, New York, 668 p.

1196 Miller, K.B., Brett, C.E. and Parsons, K. M., (1988). The paleoecologic significance of
1197 storm-generated disturbance within a middle Devonian muddy epeiric sea. *Palaios*,
1198 3:35-52.

1199 Miller, K. G. and Gornitz, V., (2008).” Sea level change, last 250 million years,” in
1200 *Encyclopedia of Paleoclimatology and Ancient Environments*, V. Gornitz, Ed., vol. 1 of
1201 *Encyclopedia of Earth Sciences Series*, pp. 879–887, Springer, Dordrecht.

1202 Mount, J. (1985). Mixed siliciclastic and carbonate sediments: a proposed first-order
1203 textural and compositional classification. *Sedimentology*, 32(3), 435-442.

1204 Mulder, T., Alexander, J. 2001. The physical character of subaqueous sedimentary
1205 density flow and their deposits. *Sedimentology*, 48(2), 269–299.
1206 <https://doi.org/10.1046/j.1365-3091.2001.00360>.

1207 McCubbin, D. G. (1982). Barrier-island and strand plain facies. In: Scholle P.A. and
1208 Spearing D. *Sandstone Depositional Environments*, Tulsa, Oklahoma, The American
1209 Association of Petroleum Geologists, p. 247-279.

1210 Mclaughlin, Patrick I. Brett Carlton E.; Signatures of sea-level rise on the carbonate
1211 margin of a late Ordovician Foreland Basin: A case study from the Cincinnati Arch, USA.
1212 *Palaios*, 2007; 22 (3): 245–267.

1213 Myrow, P. M., Southard, J. B., (1999). Combined-flow model for vertical stratification
1214 sequences in shallow marine storm-deposited beds. *Journal of Sedimentary Petrology*,
1215 61(2), 202–210.

1216 Myrow, P., (2005). Storms and Storm Deposits. In *Encyclopedia of Geology* (Issue
1217 February). Elsevier Inc. <https://doi.org/10.1016/b978-0-12-409548-9.09736-0>

1218 Naish, T. R. and Kamp, P. J. J. (1997). High-resolution sequence stratigraphy of 6 th order
1219 (41 ka) Plio-Pleistocene cyclothems, Wanganui Basin, New Zealand. *Bulletin of the*
1220 *Geological Society of America*, 109, 978-999.

1221 Natland, M. L., (1974). A System of Stages for Correlation of Magallanes Basin.
1222 *Sediments* (Vol. 139). Geological Society of America.

1223 Naylor, M., and Sinclair, H. D. (2008). Pro- vs. retro-foreland basins: Basin Research,
1224 20, p. 285–303.

1225 Nemec, W. and Steel, R. J., (1984). In: ‘Sedimentology of Gravels & Conglomerates’.
1226 (Ed. By E.H. Koster and R.J. Steel). (1984). Alluvial and coastal conglomerates: their
1227 significant features and some comments on gravelly mass-flows. *Can. Soc. Petrol. Geol.*,
1228 *Memoir 10*, p. 1-31, *Memoir 10*(January), 1–31.

1229 Nichols, G., (2009). *Sedimentology and Stratigraphy*. Blackwell Publishing, A John
1230 Wiley & Sons, Ltd., Publication, 432P.

1231 Nizou, J. Hanebuth, T. J. J., Heslop, D., Schwenk, T., Palamenghi, L., Stuut, J. B.,
1232 Henrich, R., (2010). The Senegal River mud belt: A high-resolution archive of
1233 paleoclimatic change and coastal evolution. *Mar Geol* 278:150–164. doi:
1234 10.1016/j.margeo.2010.10.002

1235 Nullo, F., and Combina, A., (2011).”Patagonian continental deposits (Cretaceous-
1236 Tertiary)”. *Biological Journal of the Linnean Society*, vol. 103, no. 2, pp. 289–304.

1237 Ori, G.G., Roveri, M. and Vannoni, F., (1986). Plio–Pleistocene Sedimentation in the
1238 Apenninic–Adriatic Foredeep (Central Adriatic Sea, Italy). In *Foreland Basins* (eds P.A.
1239 Allen and P. Homewood). <https://doi.org/10.1002/9781444303810.ch9>
1240 Payros, A., Ortiz, S., Alegret, L., Orue-Etxebarria, X., Apellaniz, E., and Molina, E.,
1241 (2012). An early Lutetian carbon-cycle perturbation: Insights from the Gorrondatxe
1242 section (western Pyrenees, Bay of Biscay). *Paleoceanography*. 27.
1243 10.1029/2012PA002300.

1244 Pilger, R. H., (1983). Kinematics of the South American subduction zone from global plate
1245 reconstructions, In: *Geodynamics of the Eastern Pacific Region, Caribbean and Scotia*
1246 *Arcs*, *Geodynamics Series*, 9: 113-125.

1247 Parras, A., and Casadío, S., (2005). Taphonomy and sequence stratigraphic significance
1248 of oyster-dominated concentrations from the San Julián formation, Oligocene of
1249 Patagonia, Argentina. *Palaeogeography, Palaeoclimatology, Palaeoecology*, 217(1–2),
1250 47–66. <https://doi.org/10.1016/j.palaeo.2004.11.015>

1251 Patzkowsky, M. E., and Holland, S. M., (2012). *Stratigraphic paleobiology.*
1252 *Understanding the distribution of fossil taxa in time and space.* The University of Chicago
1253 Press. Chicago, USA, 256 p.

1254 Pemberton, S. G., Spila, M., Pulham, A. J., Saunders, T., MacEachern, J. A., Robbins,
1255 D., and Sinclair, I. K., (2001). *Ichnology and sedimentology of shallow to marginal*
1256 *marine systems.* Geological Association of Canada, Short Course Notes 15, 343 pp.

1257 Pemberton, S.G., MacEachern, J.A., and Saunders, T., (2004). Stratigraphic applications
1258 of substrate-specific ichnofacies: delineating discontinuities in the rock record. In:
1259 McIlroy, D. (Ed.), *The Application of Ichnology to Palaeoenvironmental and*
1260 *Stratigraphic Analysis.* Special Publication, 228 Geological Society of London, pp. 29–
1261 62.

1262 Pemberton, S. G., Maceachern, J. A., Dashtgard, S. E., Bann, K. L., Gingras, M. K., and
1263 Zonneveld, J., (2012). Shorefaces (Vol. 64).

1264 Pearson, N. J., Mángano, M. G., Buatois, L. A., Casadío, S., Raising, M. R., (2012).
1265 Ichnology, sedimentology, and sequence stratigraphy of outer-estuarine and coastal-plain
1266 deposits: Implications for the distinction between allogenic and autogenic expressions of
1267 the Glossifungites Ichnofacies. *Palaeogeography, Palaeoclimatology, Palaeoecology*,
1268 333, 192-217.

1269 Plint, A. G., (2010). Wave- and storm-dominated shoreline and shallow marine systems.
1270 In: James N.P., Dalrymple R. W. (Eds.), *Facies models 4. Newfoundland & Labrador*,
1271 *Geological Association of Canada Publications*, 4, p. 167-199.

1272 Puga-Bernabéu, Á., Aguirre, J. (2017). Contrasting storm-versus tsunami-related shell
1273 beds in shallow-water ramps. *Palaeogeography, Palaeoclimatology, Palaeoecology*, 471,
1274 1-14.

1275 Quaglio, F., Warren, L. V., Anelli, L. E., Dos Santos, P. R., Rocha-Campos, A. C.,
1276 Gaździcki, A., Strikis, P. C., Ghilardi, R. P., Tiozzi, A. B., & Simões, M. G., (2014). Shell
1277 beds from the Low Head Member (Polonez Cove Formation, early Oligocene) at King
1278 George Island, west Antarctica: New insights on facies analysis, taphonomy and
1279 environmental significance. *Antarctic Science*, 26(4), 400–412.

1280 Ramos, V., Cristallini E. O., and Pérez D. J. (2002) The Pampean flat-slab of the central
1281 Andes. *Journal of South America Earth Science*, 15:59–78

1282 Reading, H. G., Collinson, J. D., (1996). Clastic coast. In: Reading, H. G. (Ed.),
1283 *Sedimentary Environment: Processes, Facies and Stratigraphy*. Blackwell Publ., pp. 154–
1284 231.

1285 Rigueti, A. L., Dal’Bó, P. F., Borghi, L., & Mendes, M. (2020). Bioclastic accumulation
1286 in a lake rift basin: The Early Cretaceous coquinas of the Sergipe-Alagoas Basin, Brazil.
1287 *Journal of Sedimentary Research*, 90(2), 228–249. <https://doi.org/10.2110/jsr.2020.11>
1288 Richardson, E. S. and Rona, P. A., (1980). Global Eocene plate reorganization:
1289 implications for petroleum exploration. In: ESCAP, CCOP/SOPAC. p. 25-36. (Tech.
1290 Bull. 3).

1291 Rivera, H. A., Roux, J. P., Le, Fariás, M., Gutiérrez, N. M., Sánchez, A., Palma-heldt, S.
1292 and Celle, L. (2020). Tectonic controls on the Maastrichtian-Danian transgression in the
1293 Magallanes-Austral foreland basin (Chile): Implications for the growth of the Southern
1294 Patagonian Andes, *Sedimentary Geology*, Volume 403,2020,105645,ISSN 0037-
1295 0738,<https://doi.org/10.1016/j.sedgeo.2020.105645>

1296 Rothwell, R. G., Hoogakker, B., Thomson, J., Croudace, I. W., Frenz, M. (2006).
1297 Turbidite emplacement on the southern Balearic Abyssal Plain (western Mediterranean
1298 Sea) during Marine Isotope Stages 1–3: an application of ITRAX XRF scanning of
1299 sediment cores to lithostratigraphic analysis. In: Rothwell RG (ed) *New Techniques in*
1300 *Sediment Core Analysis*. *Geol Soc Spec Publ* 267:79–98. doi:10.1144/
1301 GSL.SP.2006.267.01.06

1302 Rossetti, D. F. (1997). Internal architecture of mixed tide- and storm-influenced deposits:
1303 An example from the Alcântara Formation, northern Brazil. *Sedimentary Geology*,
1304 114(1–4), 163–169. [https://doi.org/10.1016/S0037-0738\(97\)00067-5](https://doi.org/10.1016/S0037-0738(97)00067-5). *Res.*, 60, 211–
1305 219.

1306 Royer, D. (2006). CO₂-forced climate thresholds during the Phanerozoic. *Geochimica et*
1307 *Cosmochimica Acta*. 70. 5665-5675. [10.1016/j.gca.2005.11.031](https://doi.org/10.1016/j.gca.2005.11.031)

1308 Samira, T. N., Payman, R., Reza, M. H., & Mohammad, K. (2018). Shell concentrations
1309 analysis in the Lower Permian carbonate rocks (Khan Formation) in Central Iran

1310 (Kalmard area). In *Historical Biology* (Issue October).
1311 <https://doi.org/10.1080/08912963.2018.1539969>

1312 Sames, B., Wagreich, M., Conrad C., and Iqbal S., (2020). Aquifer-eustasy as the main
1313 driver of short-term sea-level fluctuations during Cretaceous hothouse climate phases. In:
1314 Wagreich M., Hart M.B., Sames B. & Yilmaz I.O. (eds) *Cretaceous Climate Events and*
1315 *Short-Term Sea-Level Changes*. Geological Society, London, Special Publications, 498.
1316 First published online February 4, 2020, <https://doi.org/10.1144/SP498-2019-105>.

1317 Seilacher, A., (1967). Bathymetry of trace fossils. *Marine Geology*, 5, 413–428.

1318 Simões, M. G., and Kowalewski, M., (1998). Shell beds as paleoecological puzzles:a case
1319 study from the upper permian of the parana basin, Brazil. In *Facies* (Issue 38, pp. 175–
1320 196). <https://doi.org/10.1007/bf02537364>

1321 Simões, M. G., and Torello, F. D. F. (2003). Modelo de tafofácies para os moluscos
1322 bivalves do Grupo Passa Dois (Formações Serra Alta, Teresina E Corumbataí), Permiano
1323 Superior, Bacia Do Paraná, Brasil. *Revista Brasileira de Geociências*, 33(4), 369–378.
1324 <https://doi.org/10.25249/0375-7536.2003334369378>

1325 Shoup, E., (2001). Sedimentology and taphonomy of a shell bed assemblage from the
1326 Upper Cretaceous (Maastrichtian) Hell Creek Formation of eastern Montana. 66

1327 Schwartz, T.M., and Graham, S.A. (2015). Stratigraphic Architecture of a Tide-
1328 Influenced Shelf-Edge Delta, Upper Cretaceous Dorotea Formation, Magallanes-Austral
1329 Basin, Patagonia. *Sedimentology* 62(4), 1039-1077.

1330 Schwartz, T.M., Fosdick, J.C., Graham, S.A., (2016). Using Detrital Zircon U-Pb Ages
1331 to Calculate Late Cretaceous Sedimentation Rates in the Magallanes-Austral Basin,
1332 Patagonia. *Basin Research* 29(6), 725-746.

1333 Scher, H. D., and Martin, E. E., (2006). Timing and climatic consequences of the opening
1334 of Drake Passage. *Science*, 312, 428– 430.

1335 Speyer, S. E., and Brett, C. E. (1986). Trilobite taphonomy and Middle Devonian
1336 taphofacies. *Palaios*, 1(3), 312-327.

1337 Speyer, S. E., Brett, C. E. (1988). Taphofacies Models for Epeiric Sea Environments:
1338 Middle Paleozoic Examples. *Palaeogeography, Palaeoclimatology, Palaeoecology*, 63(1-
1339 3), 225-262.

1340 Spofforth, D. J. A., Pälke, H., Green, D. (2008). Paleogene record of elemental
1341 concentrations in sediments from the Arctic Ocean obtained by XRF analyses.
1342 *Paleoceanography* 23:PA1S09. doi:10.1029/2007PA001489

1343 Swift, D. J. P., Hudelson, P. M., Brenner, R. L., and Thompson, P. (1987). Shelf
1344 construction in a foreland basin: storm beds, shelf sandbodies, and shelf-slope
1345 depositional sequences in the Upper Cretaceous Mesaverde Group, Book Cliffs, Utah.
1346 *Sedimentology*, 34(3), 423–457. <https://doi.org/10.1111/j.1365-3091.1987.tb00578>.

1347 Taylor, A.M., Goldring, R., Gowland, S. (2003). Analysis and application of ichnofabric.
1348 *Earth-Sci. Rev.* 60, 227–25.

1349 Tomašových, A., (2006). Linking taphonomy to community-level abundance: Insights
1350 into compositional fidelity of the Upper Triassic shell concentrations (Eastern Alps),
1351 *Palaeogeography, Palaeoclimatology, Palaeoecology* 235(4). 0–381. doi:10.1016/j.palaeo.2005.11.005

1352 Thomson, J., Crudeli, D., De Lange, G., Slomp, C. P., Erba E., Corselli C., Calvert S. E.
1353 (2004). *Florisphaera profunda* and the origin and diagenesis of carbonate phases in eastern
1354 Mediterranean sapropel units. *Paleoceanography* 19:PA3003.
1355 doi:10.1029/2003PA000976

1356 Thomson, J., Croudace, I. W., Rothwell, R. G., (2006). A geochemical application of the
1357 ITRAX scanner to a sediment core containing eastern Mediterranean sapropel units. In:
1358 Rothwell RG (ed) *New Techniques in Sediment Core Analysis*. Geol Soc Spec Publ
1359 267:65–77. doi:10.1144/ GSL.SP.2006.267.01.05

1360 Ugalde R. A., (2014). Contribución al conocimiento de la estratigrafía cenozoica de la
1361 Sierra Baguales: La Formación Man Aike (“Las Flores”), [Undergraduate thesis],
1362 Universidad de Chile, Provincia de Última Esperanza, Magallanes

1363 Uliana, M. A., and Biddle, K. T. (1988). Mesozoic-Cenozoic Paleogeographic and
1364 Geodynamic Evolution of Southern South America. *Revista Brasileira de Geociências*,
1365 18(2), 172–190. <https://doi.org/10.25249/0375-7536.1988182172190>

1366 Van de Meene, J. W. H., Boersma, J. R., and Terwindt, J. H. J. (1996). Sedimentary
1367 structures of combined flow deposits from the shoreface-connected ridges along the
1368 central Dutch coast. *Marine Geology*, 131(3–4), 151–175.

1369 Varela, A. N., Richiano, S., Paz, D. M., Tettamanti, C., Poiré, D. G. (2019).
1370 Sedimentology and stratigraphy of the Puesto El Moro Formation, Patagonia, Argentina:
1371 Implications for upper cretaceous paleogeographic reconstruction and
1372 compartmentalization of the Austral-Magallanes Basin. *Journal of South American Earth
1373 Sciences*, 92, 466-480.

1374 Velde, B. (2014) *Green Clay Minerals*. Editor(s): Heinrich D. Holland, Karl K. Turekian,
1375 *Treatise on Geochemistry (Second Edition)*, Elsevier, 2014, Pages 351-364. ISBN
1376 9780080983004

1377 Vogt, M., Leppe, M., Stinnesbeck, W., Jujihara, T., Mansilla, H., Ortiz, H., Manríquez,
1378 L., and González, E., (2014). Depositional Environment of Maastrichtian (Late
1379 Cretaceous) Dinosaur-Bearing Deltaic Deposits of the Dorotea Formation, Magallanes
1380 Basin, Southern Chile. *The 23rd Latin American Colloquium on Earth Sciences*: 1-2.

1381 Wentworth, C.K. 1922. A scale of grade and class terms for clastic sediments. *J. Geol.* 30
1382 (5), 377–392.

1383 Wilson, T. (1991). Transition from Back Arc to Foreland Basin Development in the
1384 Southern Andes: Stratigraphic Record from the Ultima Esperanza District, Chile.
1385 Geological Society of America Bulletin 103, 98-111.

1386 Wang M., Zheng H, Xie X., Fan D., Yang S, Zhao Q., and Wang K. (2011). A 600-year
1387 flood history in the Yangtze River drainage: comparison between a subaqueous delta and
1388 historical records. *Chin Sci Bull* 56:188–195. doi: 10.1007/s11434-010-4212-2

1389 Weltje, G. J., and von Eyhatten, H., (2004). Quantitative provenance analysis of
1390 sediments: review and outlook. *Sedimentary Geology*, 171, 1-11

1391 Westerhold, T., Röhl, U. D. B., Frederichs, T., Kordesch, W., Bohaty, S., Hodell, D.,
1392 Laskar, J., and Zeebe, R. (2017). Late Lutetian Thermal Maximum: Crossing a Thermal
1393 Threshold in Earth's Climate System?. *Geochemistry, Geophysics, Geosystems*. 19.
1394 10.1002/2017GC007240.

1395 Wilf, P., Johnson, K. R., Cúneo, N. R., Smith, M. E., Singer, B. S., and Gandolfo, M. A.,
1396 (2005). Eocene plant diversity at Laguna del Hunco and Río Pichileufú, Patagonia,
1397 Argentina. *American Naturalist*, 165(6), 634–650. <https://doi.org/10.1086/430055>

1398 Yang, W. (2007). Transgressive wave ravinement on an epicontinental shelf as recorded
1399 by an Upper Pennsylvanian soil-nodule conglomerate-sandstone unit , Kansas. 197, 189–
1400 205. <https://doi.org/10.1016/j.sedgeo.2006.10.002>

1401 Yokokawa, M., (1995). Combined-flow ripples: genetic experiments and applications for
1402 geologic records. *Memoirs - Kyushu University, Faculty & Science, Series D, Earth &*
1403 *Planetary Sciences*, 29(1), 1–38.

1404 Zachos, J. C., M. Pagani, L. C. Sloan, E. Thomas, and K. Billups. (2001). Trends,
1405 rhythms, and aberrations in global climate 65 Ma to present. *Science* 292:686–693

1406 Zachos, J. C., Dickens, G. R., Zeebe, R. E. (2008). An early Cenozoic perspective on
1407 greenhouse warming and carbon cycle dynamics, *Nature*, 451, 279–283.

1408 Zavala, C., Arcuri, M., Gamero, H., Contreras, C., and Di Meglio, M. (2011). A Genetic
1409 Facies Tract for the Analysis of Sustained Hyperpycnal Flow Deposits.
1410 10.1306/13271349St613438.

1411 Zavala, C., Arcuri, M., Di Meglio, M., Zorzano, A., (2014). Depósitos De Turbiditas Intra
1412 Y Extra Cuencas: Origen Y Características Distintivas. 10.13140/2.1.4603.8088.

1413 Zavala, C. (2020). Hyperpycnal (over density) flows and deposits. Journal of
1414 Palaeogeography, 9(1). <https://doi.org/10.1186/s42501-020-00065-x>

1415 Zecchin, M, and Catuneanu, O., (2013). High-resolution sequence stratigraphy of clastic
1416 shelves I: units and bounding surfaces. Mar Pet Geol 39:1–25

1417 Zecchin M., Caffau M., Catuneanu O., Lenaz, D., (2017). Discrimination between wave-
1418 ravinement surfaces and bedset boundaries in Pliocene shallow-marine deposits, Crotona
1419 Basin, southern Italy: An integrated sedimentological, micropalaeontological and
1420 mineralogical approach. Sedimentology, 64(7):1755-1791.
1421 <https://doi.org/10.1111/sed.12373>

1422

1423 SÍNTESE INTEGRADORA

1424

1425 O desenvolvimento deste estudo tafonômico-sedimentar das concentrações
1426 fossilíferas possibilitou contribuir com o conhecimento estratigráfico e paleoambiental da
1427 deposição Eocênica da Formação Man Aike na Bacia de Magallanes além de
1428 contribuições com novos *insights* sobre a abordagem e o uso destas concentrações
1429 fossilíferas. O estudo sedimentológico e tafonômico corrobora com a interpretação prévia
1430 para a base desta sequência como sendo deposição em ambiente de *shoreface* superior
1431 formado sob trato de sistema transgressivo (TST), previamente interpretado por
1432 Manríquez et al., (2019).

1433 O estudo mostrou padrões e assinaturas bem distintas na formação dessas
1434 concentrações fossilíferas. Essas concentrações se distribuem conforme a variação do
1435 nível do mar, paleogeografia e processos dinâmicos associados a costa. A análise
1436 tafonômica destas concentrações densas juntamente com a análise geoquímica de
1437 sedimentos e o controle sedimentar e petrográfico, nos permitiu caracterizar uma
1438 tendência de aprofundamento da lâmina da água e maior influência de tempestades em
1439 direção ao topo da seção. Essa variação relativa do nível do mar na região pode ser ligada
1440 a eventos climáticos que ocorreram no Lutetiano, ou processos tectônicos incidentes
1441 nessa bacia de retro foreland.

1442 Três tipos de concentrações foram registrados. Concentrações de *lags*, ligadas a
1443 subida de nível do mar e início de transgressões. Essas concentrações estão associadas a
1444 regiões mais proximais a costa (Upper Shoreface). Concentrações de episódicas de *debris*
1445 *flows* gerando depósitos retrabalhados, porém de soterramento rápido, para fora da Zona
1446 Tafonomicamente Ativa (TAZ). E por fim, concentrações hiatais com evidências de *event*
1447 *concentration*, ou associações de censo ecológico, aqui interpretadas causados por
1448 tempestades em regiões mais distais gerando depósitos de soterramento rápido marcado
1449 por pavimentos de conchas.

1450 Devido a variação e complexidade do balanço entre sedimentação, processos
1451 biológicos, paleogeografia e influência de fatores externos a bacia de sedimentação, mais
1452 estudos são necessários nesse período para melhor compreensão da relação eustasia e
1453 eventos costeiros atuantes durante a formação e deposição das concentrações fossilíferas
1454 da Formação Man Aike.

1455

1456 **REFERÊNCIAS**

- 1457 Aagaard, T., Greenwood, B., and Hughes, M. (2013). Sediment transport on dissipative,
1458 intermediate, and reflective beaches. *Earth-Science Reviews*, 124, 32–50.
1459 <https://doi.org/10.1016/j.earscirev.2013.05.002>
- 1460 Anderson, L., and McBride, R. (1996). Taphonomic and Paleoenvironmental Evidence
1461 of Holocene Shell-Bed Genesis and History on the Northeastern Gulf of Mexico Shelf.
1462 *PALAIOS*, 11(6), 532-549. doi:10.2307/3515189
- 1463 Beckvar, N., Kidwell, S. M. 1988. Hiatal shell concentrations, sequence analysis, and
1464 sealevel history of a Pleistocene coastal alluvial fan, Punta Chueca, Sonora. *Lethaia*,
1465 21(3), 257-270.
- 1466 Brett, Carlton E. Hendy, Austin J.W. Bartholomew, Alex J. Bonelli, James R.
1467 McLaughlin; Patrick I. (2007). Response of Shallow Marine Biotas to Sea-Level
1468 Fluctuations: A Review of Faunal Replacement and The Process Of Habitat Tracking.
1469 *Palaios*; 22 (3): 228–244.
- 1470 Cattaneo, A., and Steel, R. J. (2003). Transgressive deposits: A review of their variability.
1471 *Earth-Science Reviews*, 62(3–4), 187–228. [https://doi.org/10.1016/S0012-](https://doi.org/10.1016/S0012-8252(02)00134-4)
1472 [8252\(02\)00134-4](https://doi.org/10.1016/S0012-8252(02)00134-4)
- 1473 Cuitiño, J. I., Varela, A. N., Ghiglione, M. C., Richiano, S., and Poiré, D. G. 2019. The
1474 Austral-Magallanes Basin (southern Patagonia): A synthesis of its stratigraphy and
1475 evolution. *Latin American Journal of Sedimentology and Basin Analysis*, 26(2), 155–
1476 166.
- 1477 Dickinson, W.R. (1985). Interpreting provenance relations from detrital modes of
1478 sandstones. In: Zuffa, G.G. (Ed.), *Provenance of Arenites*. D. Reidel Publishing
1479 Company, 1985, 333-363
- 1480 Dattilo, B. F., Brett, C. E., Tsujita, C. J., and Fairhurst, R. (2008). Sediment supply versus
1481 storm winnowing in the development of muddy and shelly interbeds from the Upper
1482 Ordovician of the Cincinnati region, USA. *Canadian Journal of Earth Sciences*, 45(2),
1483 243–265. <https://doi.org/10.1139/E07-060>
- 1484 Dattilo, B. F., C. E. Brett, And T. J. Schramm. (2012). Tempestites in a teapot?
1485 Condensation-generated shell beds in the Upper Ordovician, Cincinnati Arch, U.S.A.
1486 *Palaeogeography, Palaeoclimatology, Palaeoecology*, 367–368:44–62
- 1487 Fosdick, J. C., VanderLeest, R. A., Bostelmann, J. E., Leonard, J. S., Ugalde, R., Oyarzún,
1488 J. L., and Griffin, M. (2020). Revised Timing of Cenozoic Atlantic Incursions and

1489 Changing Hinterland Sediment Sources during Southern Patagonian Orogenesis.
1490 Lithosphere, 2020(1), 1–18. <https://doi.org/10.2113/2020/8883099>

1491 García-Ramos, D. A., & Zuschin, M., 2019. High-frequency cycles of brachiopod shell
1492 beds on subaqueous delta-scale clinoforms (early Pliocene, south-east Spain).
1493 Sedimentology, 66(5), 1486–1530. <https://doi.org/10.1111/sed.12541>

1494 Holland, S.M., 2001. Sequence stratigraphy and fossils. In: Briggs, D.E.G., Crowther,
1495 P.R. (Eds.), Palaeobiology, vol. II. Blackwell Science, Oxford, pp. 548– 553.

1496 Huyghe, D., Merle, D., Lartaud F, Emilie Cheype & Laurent Emmanuel. 2012 Middle
1497 Lutetian climate in the Paris Basin: implications for a marine hotspot of paleobiodiversity.
1498 Facies 58, 587–604 (2012). <https://doi.org/10.1007/s10347-012-0307-3>

1499 Ivany, L. Lohmann, K. & Hasiuk, Franciszek & Blake, Daniel & Glass, Alexander &
1500 Aronson, Richard & Moody, Ryan., 2008. Eocene climate record of a high southern
1501 latitude continental shelf: Seymour Island, Antarctica. Geological Society of America
1502 Bulletin - GEOL SOC AMER BULL. 120. 10.1130/B26269.1.

1503 Kidwell, S. M. 1986. Models for fossil concentrations: paleobiologic implications.
1504 Paleobiology, 6-24.

1505 Marensi, S.A., Casadío, S., Santillana, S., 2002. La Formación Man Aike Al Sur De El
1506 Calafate (Provincia De Santa Cruz) Y Su Relación Con La Discordancia Del Eoceno
1507 Medio En La Cuenca Austral. Revista De La Asociación Geológica Argentina 57 (3),
1508 341-344.

1509 Marensi, S.A., Casadío, S., Santillana, S.N., 2003. Estratigrafía Y Sedimentología De
1510 Las Unidades Del Cretácico Superior-Paleógeno Aflorantes En La Margen Sureste Del
1511 Lago Viedma, Provincia De Santa Cruz, Argentina. Revista De La Asociación Geológica
1512 Argentina 58(3), 403-416.

1513 Manríquez, L. M., Lavina, E. L., Fernández, R. A., Trevisan, C., Leppe, M. A., 2019.
1514 Campanian-Maastrichtian and Eocene Stratigraphic Architecture, Facies Analysis, and
1515 Paleoenvironmental Evolution of the Northern Magallanes Basin (Chilean Patagonia).
1516 Journal of South American Earth Sciences, 93, 102-118.

1517 Mclaughlin, Patrick I., Brett Carlton E. Signatures of Sea-Level Rise on The Carbonate
1518 Margin of a Late Ordovician Foreland Basin: A Case Study From The Cincinnati Arch,
1519 USA. Palaios, 2007; 22 (3): 245–267.

1520 Parras, A., & Casadío, S., 2005. Taphonomy and sequence stratigraphic significance of
1521 oyster-dominated concentrations from the San Julián formation, Oligocene of Patagonia,

1522 Argentina. *Palaeogeography, Palaeoclimatology, Palaeoecology*, 217(1–2), 47–66.
1523 <https://doi.org/10.1016/j.palaeo.2004.11.015>

1524 Quaglio, F., Warren, L. V., Anelli, L. E., Dos Santos, P. R., Rocha-Campos, A. C.,
1525 Gaździcki, A., Strikis, P. C., Ghilardi, R. P., Tiozzi, A. B., & Simões, M. G., 2014. Shell
1526 beds from the Low Head Member (Polonez Cove Formation, early Oligocene) at King
1527 George Island, west Antarctica: New insights on facies analysis, taphonomy and
1528 environmental significance. *Antarctic Science*, 26(4), 400–412.

1529 Rigueti, A. L., Dal’Bó, P. F., Borghi, L., & Mendes, M. (2020). Bioclastic accumulation
1530 in a lake rift basin: The Early Cretaceous coquinas of the Sergipe-Alagoas Basin, Brazil.
1531 *Journal of Sedimentary Research*, 90(2), 228–249. <https://doi.org/10.2110/jsr.2020.11>

1532 Simões, M. G., & Kowalewski, M., 1998. Shell beds as paleoecological puzzles: a case
1533 study from the upper permian of the parana basin, Brazil. In *Facies* (Issue 38, pp. 175–
1534 196). <https://doi.org/10.1007/bf02537364>

1535 Ugalde R. A., 2014. Contribución al conocimiento de la estratigrafía cenozoica de la
1536 Sierra Baguales: La Formación Man Aike (“Las Flores”), [Undergraduate thesis],
1537 Universidad de Chile, Provincia de Última Esperanza, Magallanes

1538 Zecchin M, Catuneanu O., 2013. High-resolution sequence stratigraphy of clastic shelves
1539 I: units and bounding surfaces. *Mar Pet Geol* 39:1–25

1540 Simões, M. G., & Torello, F. D. F. (2003). Modelo De Tafofácies Para Os Moluscos
1541 Bivalves Do Grupo Passa Dois (Formações Serra Alta, Teresina E Corumbataí),
1542 Permiano Superior, Bacia Do Paraná, Brasil. *Revista Brasileira de Geociências*, 33(4),
1543 369–378. <https://doi.org/10.25249/0375-7536.2003334369378>

1544 Westerhold, Thomas & Röhl, Ursula & Donner, B. & Frederichs, T. & Kordesch, W. &
1545 Bohaty, S. & Hodell, D. & Laskar, J. & Zeebe, R. 2017. Late Lutetian Thermal
1546 Maximum: Crossing a Thermal Threshold in Earth's
1547
1548
1549
1550
1551
1552
1553
1554
1555

1556 **FIGURE CAPTIONS**

1557 **Figure 1** - (A) Map of Southern portion of South America with the location (red point)
1558 of the study area (Rio de las Chinas Valley, Magallanes Region, Chile). (B) Eocene
1559 deposits in the northern portion of the valley. (C) Distribution and location of the three
1560 sedimentary profiles described for the Man Aike Formation in the study area.

1561 **Figure 2** - Stratigraphic chart for the region of the Rio de las Chinas Valley (Modified
1562 from Malumián and Caramés, 1997; Pearson et al., 2012; Manriquez et al., 2019).

1563 **Figure 3** - A) Satellite imagery with the location of the Man Aike Formation outcrops
1564 described in the El Puesto locality. Three profiles were described (Profile 1, 2 and 3) and
1565 later compiled into a composite profile. Source: Source: Google Earth Pro.

1566 **Figure 4** - A) The Man Aike Formation overlapping the Dorotea Formation in the Ultima
1567 Esperanza province, Rio the Las Chinas valley, Chilean Patagonia. B) Profile 1 outcrop.

1568 **Figure 5** - Composed profile showing main sedimentary facies, boundary contacts, fossil
1569 content and geometry of the dense fossil concentration (Man Aike Formation).

1570 **Figure 6** - Upper shoreface facies observed in the sequence. (A) Inverse graded
1571 conglomerate (Gmg facies) showing diffuse trough cross -bedding (B) Massive sandstone
1572 beds (Sm facies). (C) Planar cross-bedding sandstone facies (Sp facies) and pebbly
1573 sandstones (Hsm facies). (D) Lateral expression of facies Sp, Hgm and Sm. (E) and (F)
1574 Through cross-bedding sandstones (St Facies). (G) Upper shoreface facies arrangement.

1575 **Figure 7** - Middle shoreface facies observed in the studied interval of the Man Aike
1576 Formation. (A) Swaley cross stratified sandstones (Scs facies). (B) Massive pebbly
1577 sandstones showing increasing upward trend in bioclasts close-packing (Hgmm facies).
1578 (C) Massive gravelly bioclastic sandstone (Hgm facies). (D) Massive gravelly bioclastic
1579 sandstones displaying erosive bottom boundary (Hgm facies).

1580 **Figure 8** - Geochemical analysis of the studied section of the Man Aike Formation. (A)
1581 Terrigenous elements influx. (B) Fluvial Input (runoff episodes). (C) Ti/Al- proxy for
1582 environmental energy conditions. (D) Sr/Ca-for proxy for Authigenic carbonate
1583 precipitation and shallow-water source. (E) Log (Zr/Rb) Grain-size proxy. Terrigenous
1584 (Terr) elements = Si + Al + Ti + Fe + K. The sedimentary section of samples collected in
1585 their relative stratigraphic position. Grayish red shadings indicating stratigraphic intervals
1586 characterized by proximal patterns in the sedimentary record.

1587 **Figure 9** - Types of fossil-concentrations observed in Hsm facies from Man Aike
1588 Formation. (A) Gravelly sandstone beds with coarse bioclasts and erosive boundaries,
1589 locally displaying diffuse contacts. (B) Large *Lahillia* shells (C) Highly erosive and
1590 discontinuous boundaries. (D) Shells displaying preferential concordant orientation,
1591 articulated and disarticulated *Lahillia* shells (with circles). (E) Bioclasts showing
1592 bimodal size-sorting with pectinid ranging from 2-3 cm associated with *Lahillia* shells
1593 ranging in size 7-9 cm (with circles).

1594 **Figure 10** - Types of fossil-concentrations observed in Hgmg facies of the Man Aike
1595 Formation. (A) Massive conglomeratic sandstones with dense fossil concentration. (B)
1596 Bioclasts lens accumulations in cross-view showing imbrication. (C) Clustering patterns
1597 observed in the fossil concentrations (D). Localized dense concentration with articulated
1598 bivalves. (E) Lowermost portion of the bed showing subordinated bivalve molds and
1599 arborescent skeletal types (bryozoan) (white circle).

1600 **Figure 11** - Types of fossil-concentrations observed in Hgmm facies from Man Aike
1601 Formation. (A) Discontinuous lens with pebble grained sandstone with erosive top
1602 boundary and gradational lower boundary. (B) Bivalve showing splayed valves. (C)
1603 Complex concentrations showing bioclastic close-packing increasing upward (dotted
1604 white line indicate the upper boundary). (D) Complex concentrations showing bivalved

1605 and univalved shells preserved as broken and fragmented shells with no preferential
1606 orientation. (E) Marked top boundary by articulated shells.

1607 **Figure S1** – Ichnofossil found in the Man Aike Formation. A) *Skolithos* burrow
1608 associated with Scs facies. B) *Skolithos* dwelling structure detail. C) Ichnofossil in the
1609 boundary between Hgmm and Scs facies. D) *Thalassinoides* within Scs facies.

1610 **Figure S21** - Dense concentrations fossil examples, Man Aike Formation. (A) Multi-
1611 element skeletons associated with the lowermost portion of the Hgmg facies.
1612 (B) Articulated bivalve (Hgmm facies). (C) Imbricated *Venericardia* shells within Hgmm
1613 facies. (D) Open-articulated *Lahillia*. (E) Articulated shells from the top boundary of
1614 Hgmm facies. (F) Bryozoan fragments found associated with the Hgmg facies. (G)
1615 Hummockys cross-stratification in a middle o lower shoreface environment interspersed
1616 with episodic concentrations and distal tempestites concentrations.

1617 **Figure S32** - Photomicrograph of thin-sections from samples collected directly from the
1618 shell accumulations beds. (A) Hsm facies showing poorly sorted siliciclastic grains with
1619 well-preserved twinning in FK grains (blue arrow) (cross-polarized light). (B) Hsm facies
1620 showing poorly-sorted grains, low maturity, quartz grains, feldspars, and high presence
1621 of ferruginous minerals. Calcite cementation and glauconite indicated by blue arrows
1622 (plane polarized light). (C) Hsm facies showing concave-convex contacts, calcite
1623 cementation, large volcanic rock fragments (blue arrow) (plane polarized light). (D)
1624 Hgmm facies showing volcanic rock fragments, sedimentary rock fragments and bioclasts
1625 fragments (blue arrow) and subordinated glauconite (plane polarized light). (E) Hgmm
1626 facies showing poorly-sorted siliciclastic grains, large quartz grain, well developed calcite
1627 cementation (blue arrow), volcanic and sedimentary fragments (plane polarized light). (F)
1628 Hgmm facies showing volcanic rock fragments (blue arrows) and polycrystalline quartz
1629 (cross-polarized light). (G) Hgmg facies showing closed bioclast radial ribs well

1630 preserved in poorly-sorted siliciclastic grains, large volcanic rock fragments and
1631 monocrystalline quartz, punctual contacts between grains, bioclasts infilled by the
1632 sedimentary matrix (blue arrow) (plane polarized light). (H) Hgmg facies showing poorly
1633 sorted siliciclastic grains and silicified bioclast umbo (blue arrow) (cross-polarized light).
1634 (I) Hgmg facies showing poorly sorted siliciclastic grains and well-preserved volcanic
1635 grains (blue arrow) (cross-polarized light).

1636

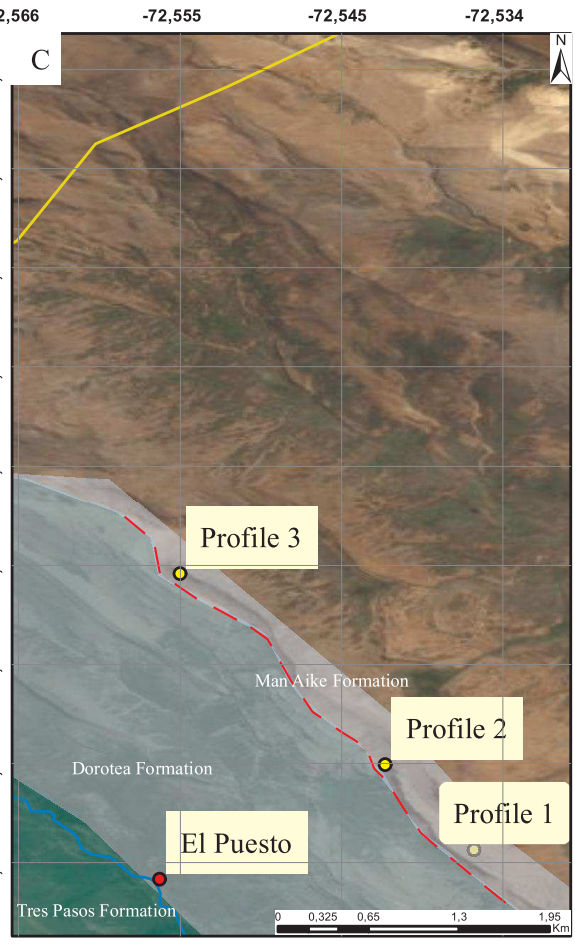
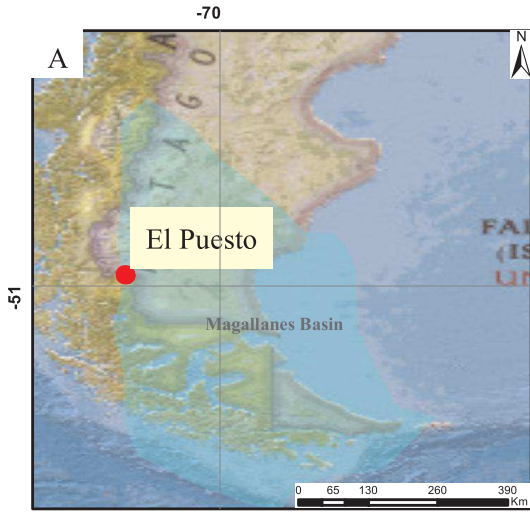
1637 **TABLE CAPTIONS**

1638 **Table 1** - Elemental ratios used as paleoenvironmental proxies.

1639 **Table 2** - Summarized facies of the Man Aike Formation.

1640

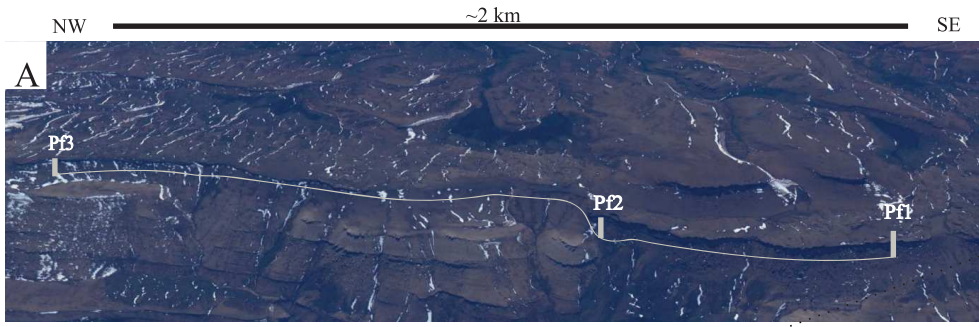
1641



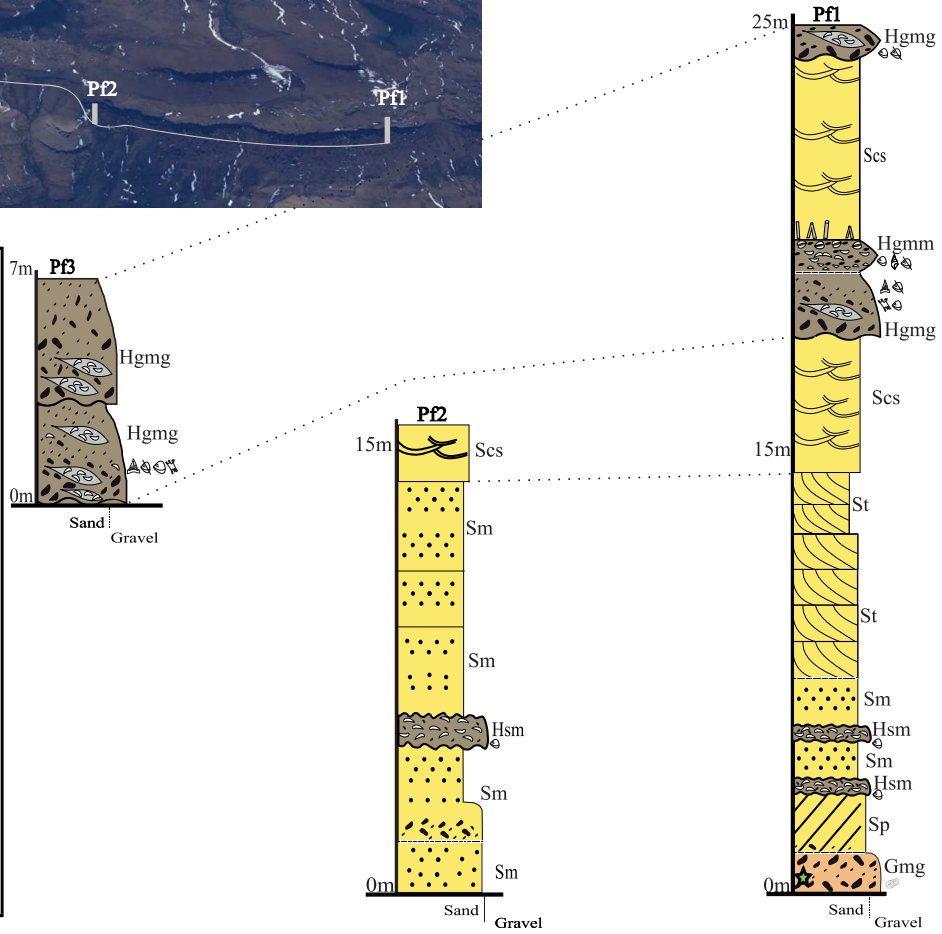
Legend



Man Aike Formation



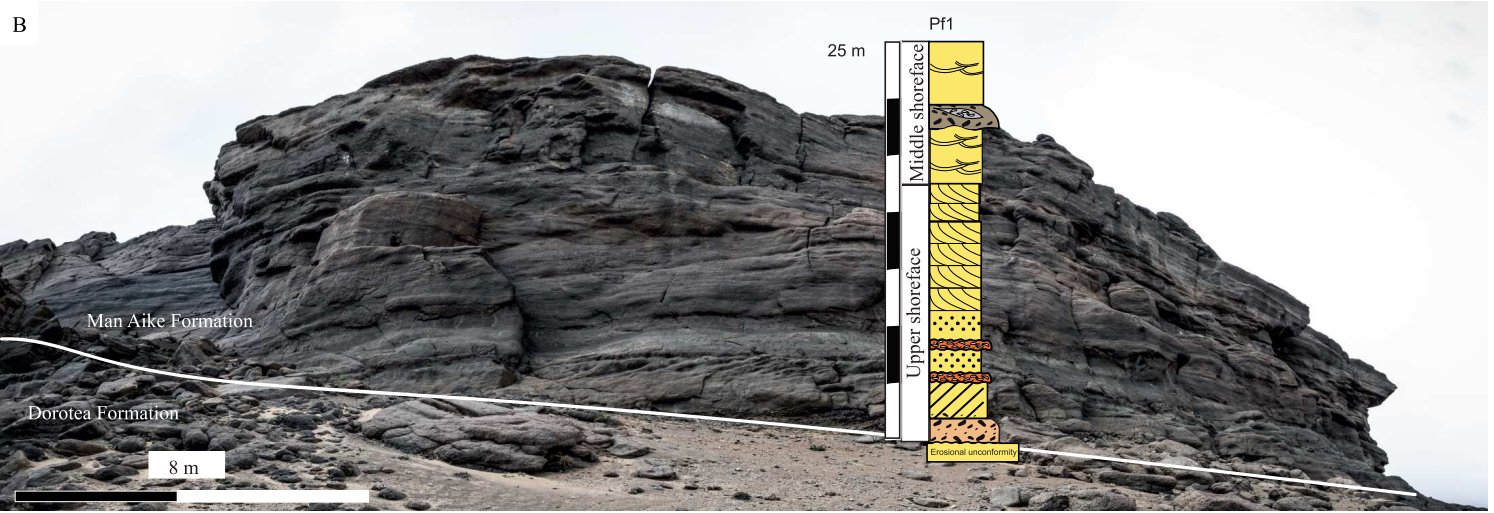
Legend	
Sedimentary structures	Lithology
Massive	Sandstone
Through cross-bedding	Pebble to Gravelly Sandstone
Planar cross-bedding	Conglomerate
Swaley cross-stratification	~ 45 Ma
Contacts	Ichonology
Abrupt/Sharp	<i>Skolithos</i>
Gradational	<i>Thalassinoides</i>
Erosive	
Shell concentration geometry	Fossil content
Lens	Gastropod
Bed	Wood
Pavements	Bivalve
Bioclasts	Shark Teeth
	Bryozoa
	Fragments

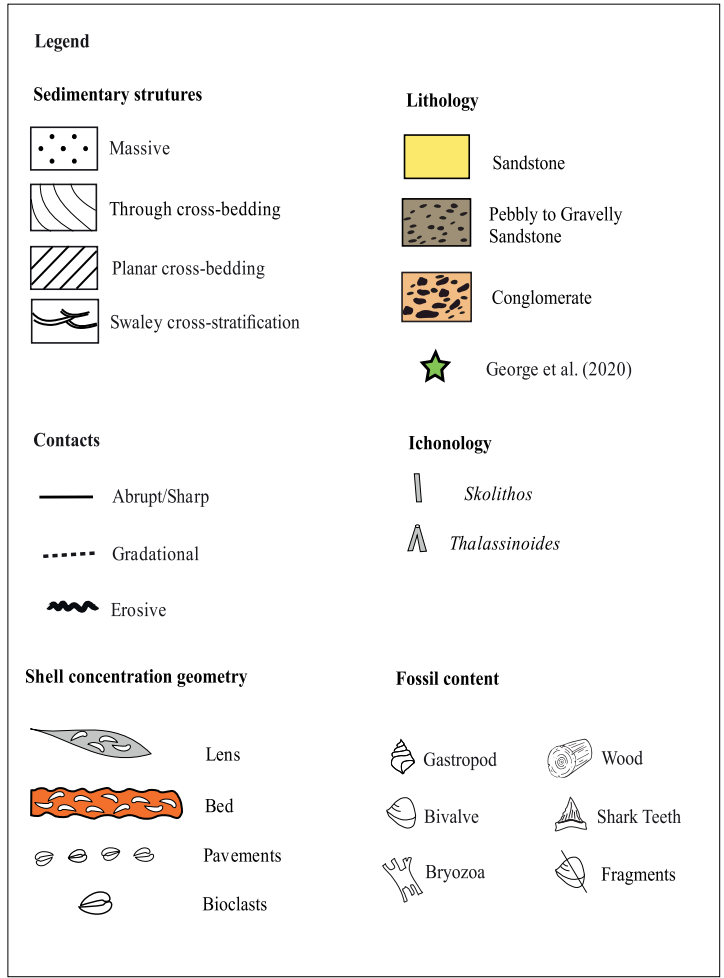
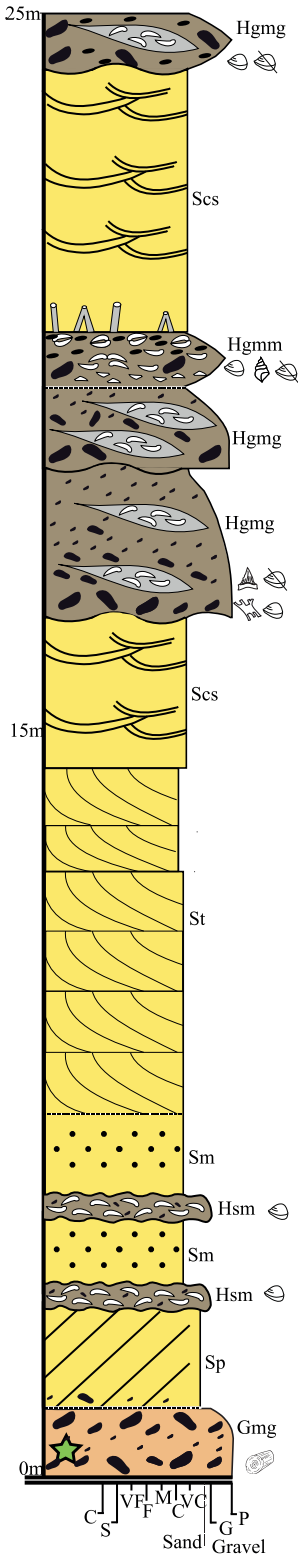


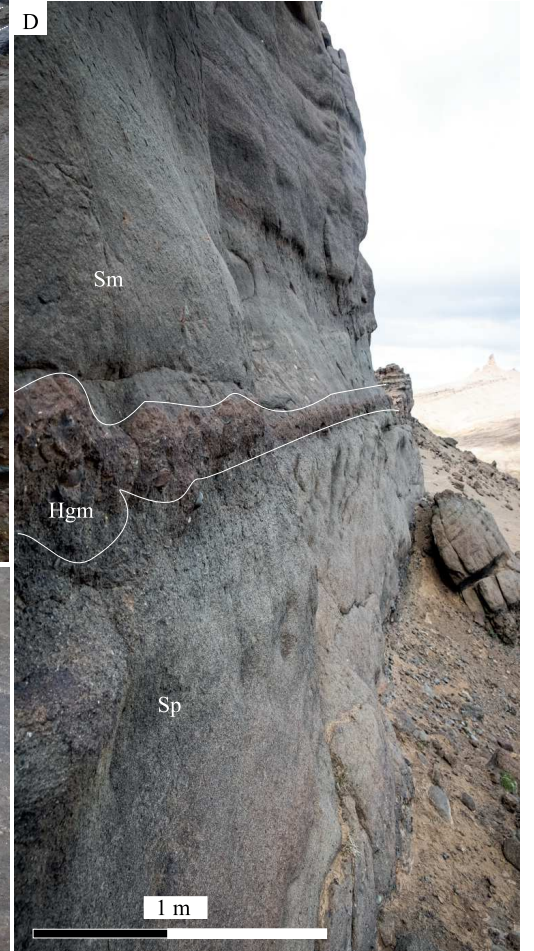
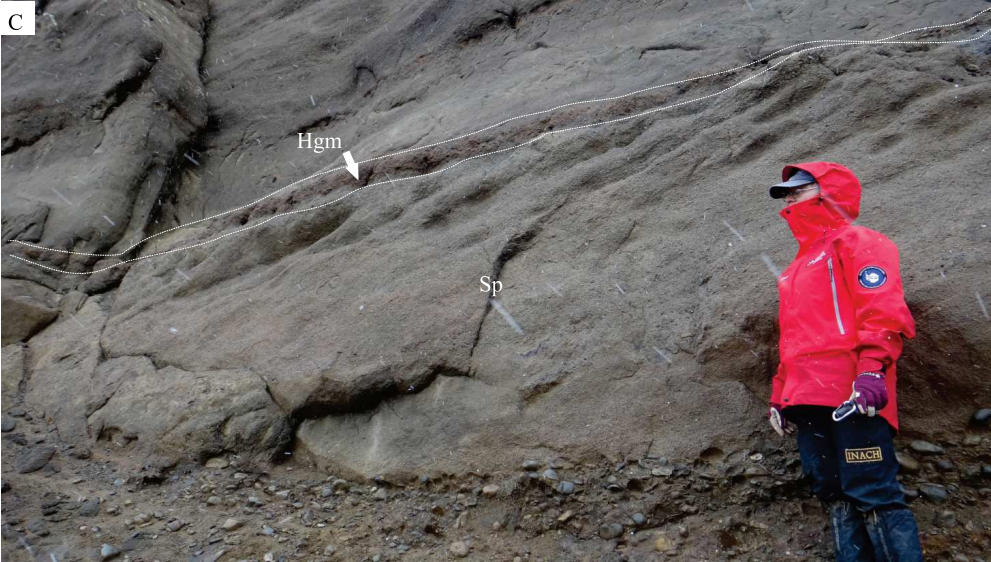
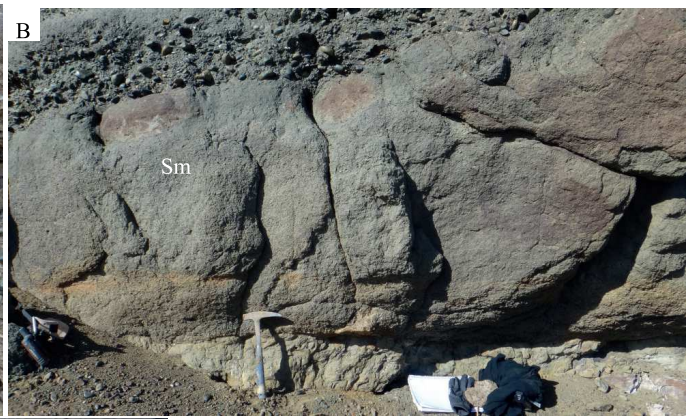
A

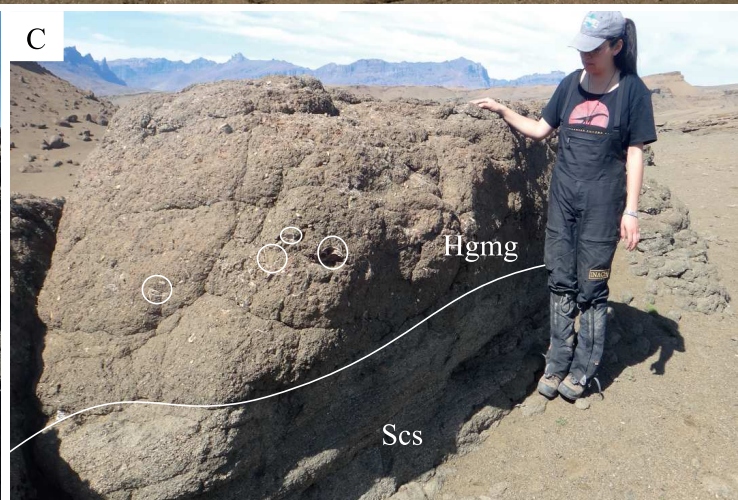
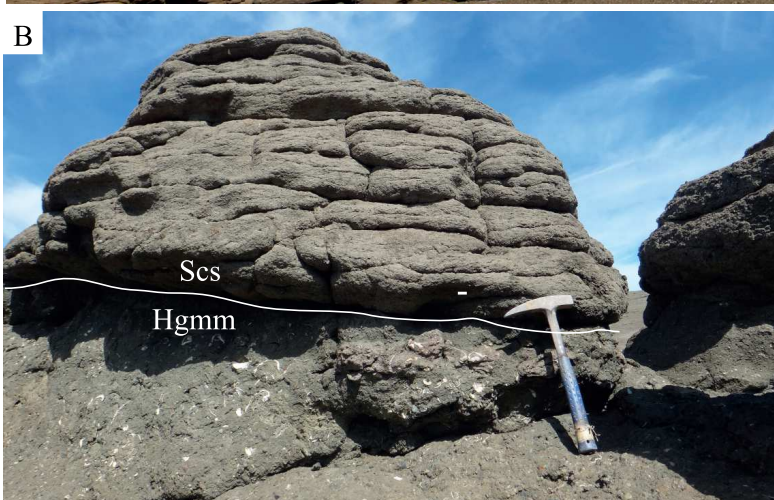


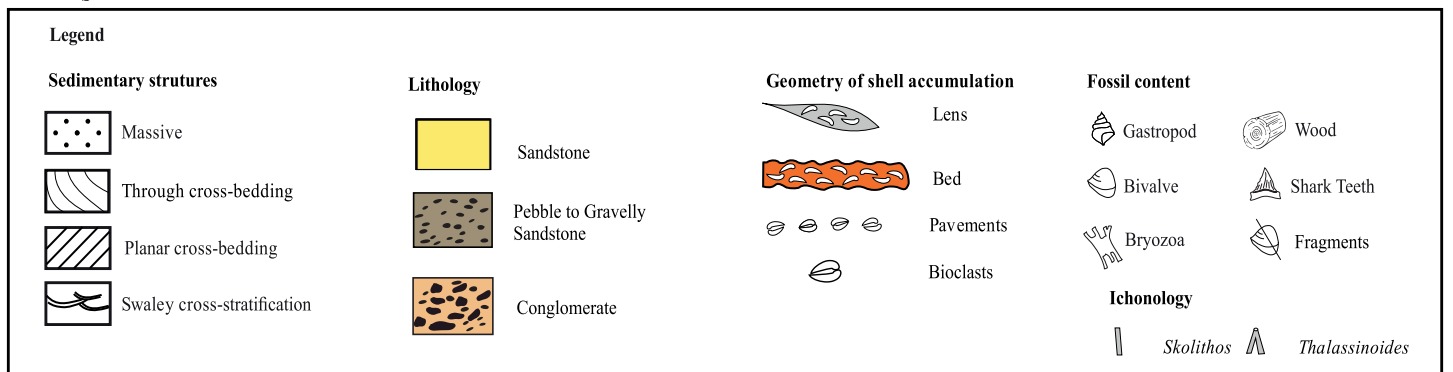
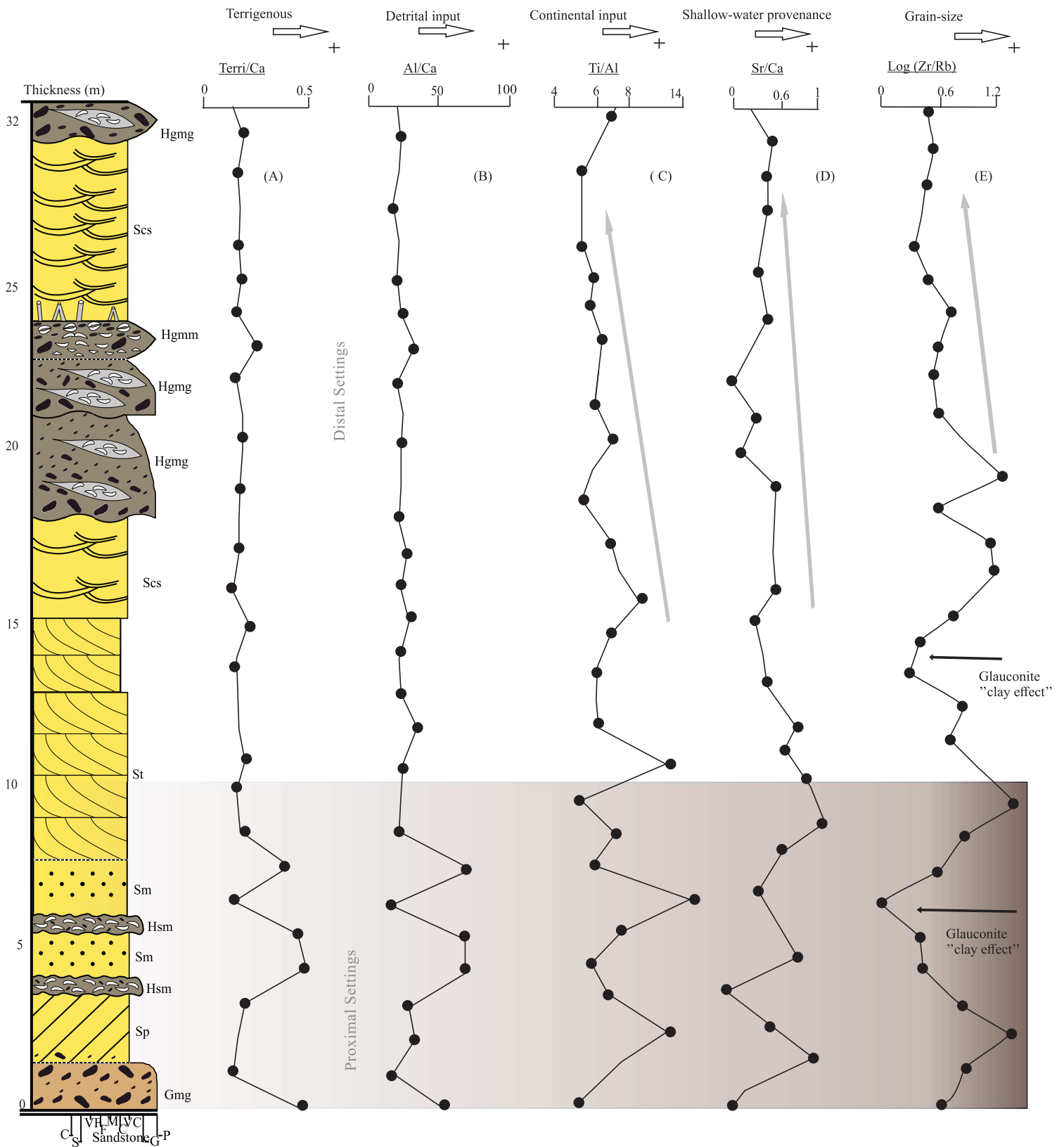
B





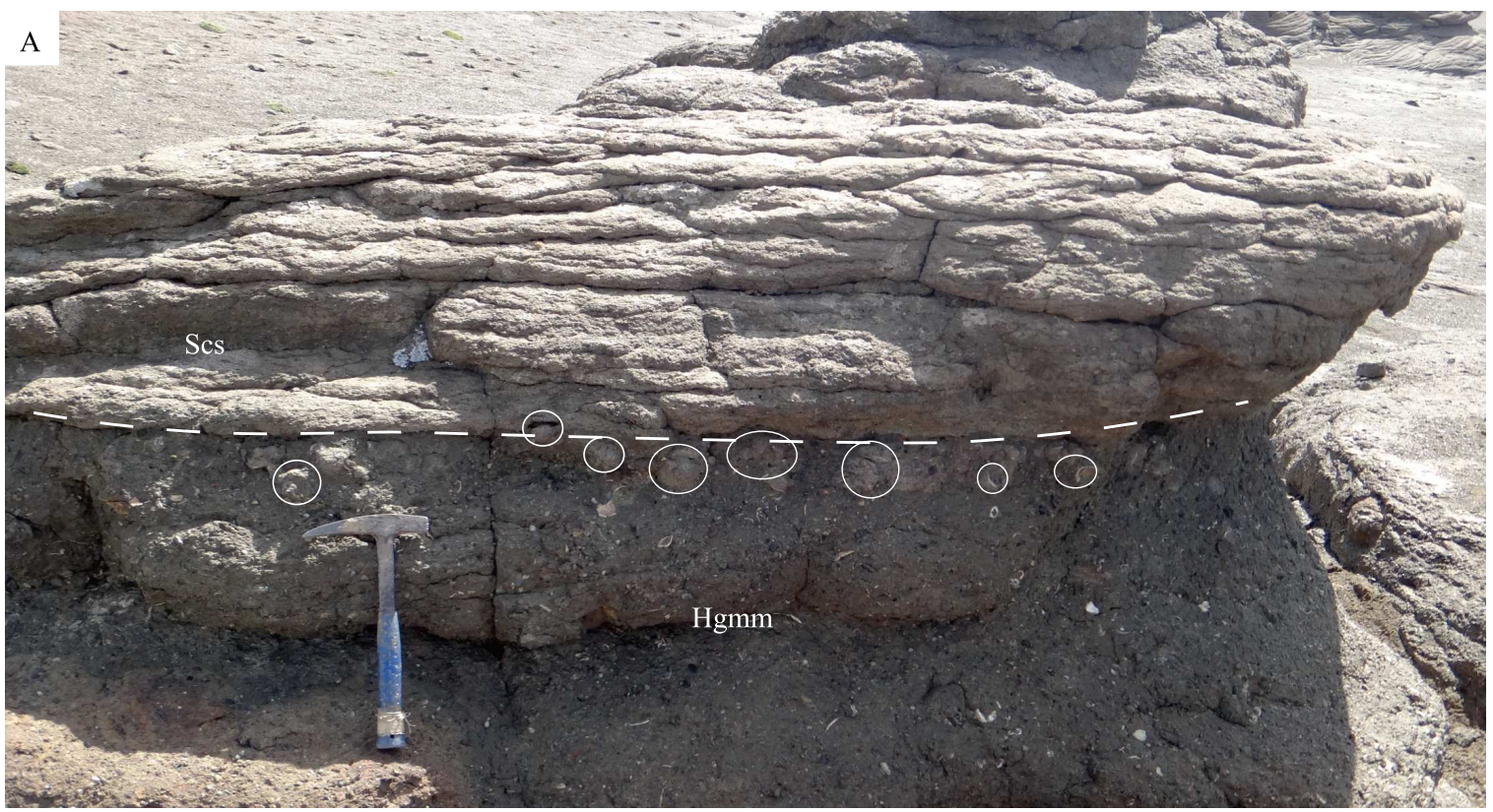


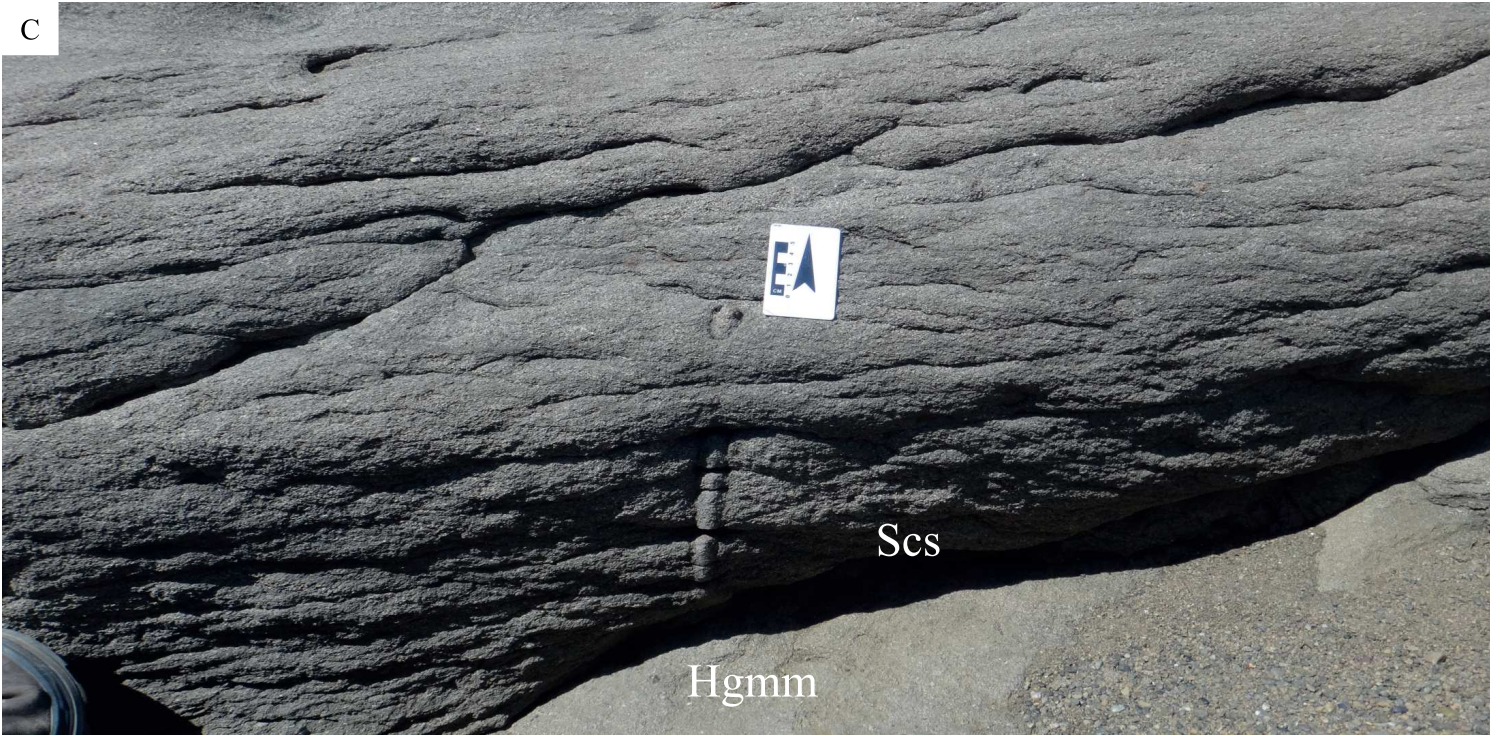
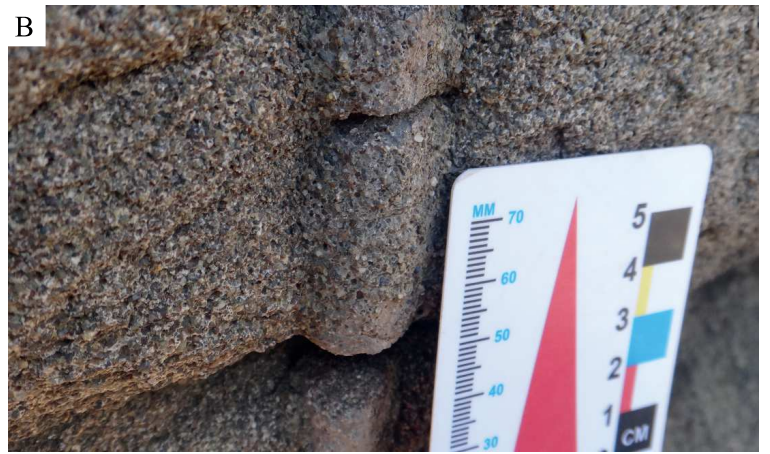


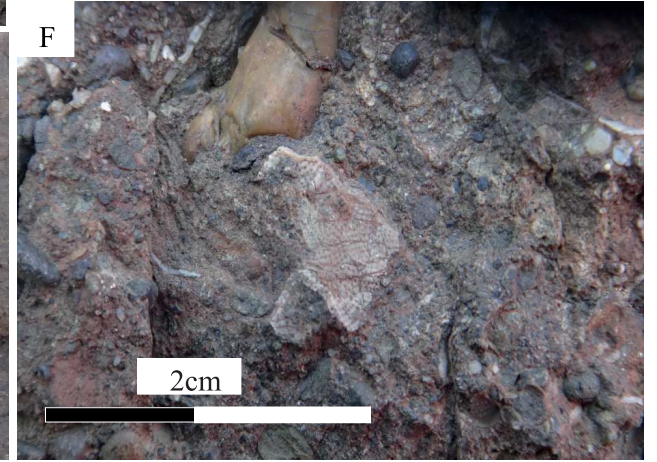












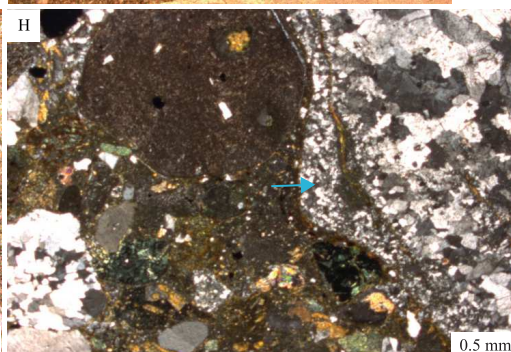
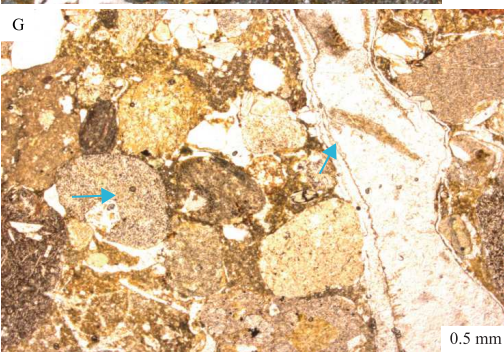
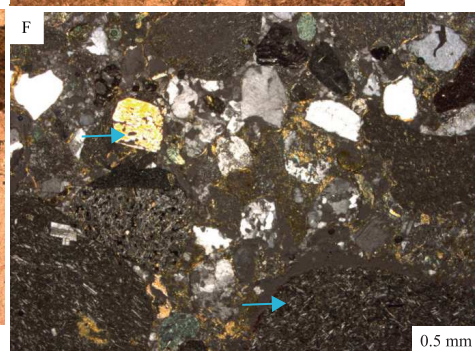
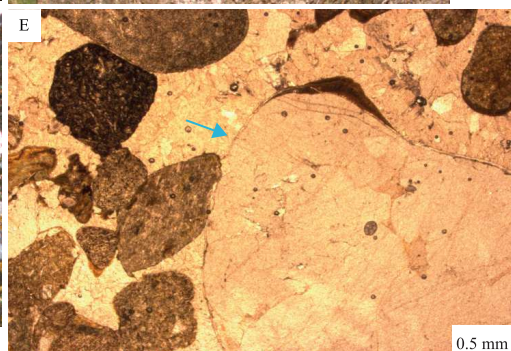
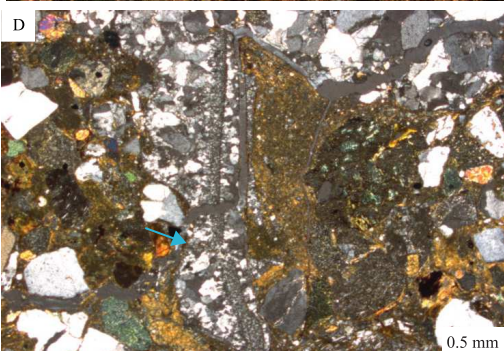
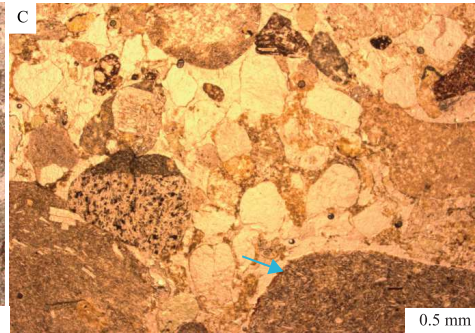
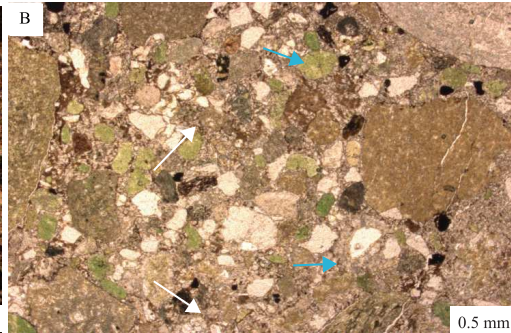
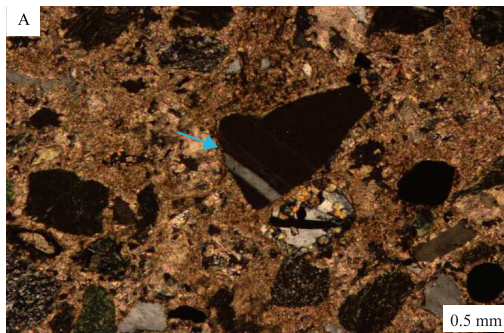


Table 1- Elemental ratios used as paleoenvironmental proxies.












Proxy	Elements	References
Terrigenous elements	Terrigenous/Ca	Bahr et al., (2008); Beil et al., (2018); Lebreiro et al., (2009)
Environmental energy	Ti/Al	Berg et al., (2010); Bourget et al. (2008); Dickson et al., (2010); Henrich et al., (2010); Itambi et al., 2009; Kwiecien et al., (2009); Chen et al., (2013)
Detrital input	Al/Ca	Nizou et al., (2010); (2011), Spofforth et al., (2008)
Shallow-water provenance	Sr/Ca	Grove et al., (2010); Rothwell et al., (2006); Thomson et al. (2006)
Grain-Size	Log (Zr/Rb)	Beil et al., (2018). Dypvik and Harris, (2001) Rothwell et al., (2006) Wang et al., (2001); Spofforth et al., (2008)

Table 2 - Summarized facies from Man Aike formation.

FACIES CODE	Description	Geometry/Dimensions	Depositional Process	Depositional environment	Fossil/Ichnofossil	Reference
Gmg	Conglomerate, clast-supported, polymictic, poorly sorted showing diffuse trough cross-bedding exhibit inverse grading, clasts imbrication. Erosive lower contact and gradational upper boundary	Tabular beds, 0.5-1.5 m thick and hundreds of meters laterally continuous.	Unidirectional current flow. Lower flow-regimes 3-D dunes	Upper shoreface	Wood Fragments	Saunders et al. (1994). Lima and Boas (1994) Reading and Collinson (1996) Clifton (2003)
Sp	Coarse to very coarse-grained sandstone with medium to large planar cross-bedding, dispersed pebbles, and granules. Gradational lower boundary and abrupt-erosive upper boundary.	Tabular laterally extensive beds, 1 – 2 m thick.	Unidirectional current flow. Lower-flow regimes 2-D dunes	Upper Shoreface	Dispersed shells	Harms et al. (1982) Allen (1963) Clifton (2006)
Sm	Massive sandstone, medium- to coarse-grained, poorly sorted, with sparse granules and pebbles.	Tabular Bed 0.5 to 1 m thick with hundreds of meters laterally extensive.	Post depositional fluidization processes or high sedimentary discharge periods	Upper shoreface	Absent	De Souza et al. (2019) Mulder and Alexander (2001) Rossi et al. (2017)
St	Medium to-coarse-grained sandstone with small trough cross-bedding showing abrupt lower and upper boundary	Tabular bed 1-2 meters thick, hundreds of meters laterally extensive, locally lenticular co-set.	Unidirectional current Lower flow regime current 3-D dunes	Upper shoreface	Absent	Allen (1963) Myrow and Southard (1999) Plint (2010)
Scs	Coarse to very coarse-grained sandstones, moderately sorted, swaley cross-stratification, Abrupt to erosive boundaries and subordinated hummockys cross-stratification	Discontinuous lenticular beds, 2 to 7 m thick and hundreds of meters wide.	Combined oscillatory and unidirectional flow generated by storm	Middle shoreface - Lower shoreface	<i>Skolithos</i> isp <i>Thalassinoides</i> isp.	Arnott and Southard (1990) Duke (1985, 1987) Duke et al (1991) Dumas and Arnott (2006)

Hsm	Massive gravelly sandstone with very coarse matrix, calcite cementation, carbonate, and ferric concretion. Bioclasts (25%) exhibiting bimodal size-sorted, with 3 and 9 (cm). Highly erosive boundaries.	Beds 0.5 m thick, hundreds of meters laterally extensive.	Wave reworking	Upper shoreface	Bivalved (<i>Lahillia</i>) Small Pectinaceous	Hart and Plint (1995) Cattaneo and Steel (2003) Zecchin et al. (2017) Kern et al. (2019)
Hgmg	Gravelly bioclastic sandstone, normally graded very-coarse grained matrix ranging grain to matrix-supported. Laterally grade to coarse grained sandstones showing cross bedding. Bioclasts (10%) poorly sorted, size ranging from 3 – 10 (cm)	Wedges 1 – 6-m thick, hundreds to thousands of meters wide	Unidirectional concentrated flow generated by debris flows	Middle-Lower - shoreface	Bivalved (Pectinaceous, <i>Lahillia</i>) Multielements (Bryozoans, Shark teeth, Corals)	Lowe (1979, 1982) Conti et al. (2019) Zavala (2020)
Hgmm	Pebbly sandstone, massive to diffuse wavy bedding with coarse grained matrix, calcite cementation, carbonate, and ferric concretion. Bioclasts (15%) are poorly sorted, size range about 3 – 7 (cm) and show content increasing upward the bed	Discontinuous lens, 0.5-1.5 meters thick and 2 -4 meters wide	Oscillatory and unidirectional flow generated by storms	Middle-Lower shoreface	Univalved (Gastropod) Bivalved (Pectinids)	Clifton (2003) Plint (2010) Amorim et al. (2020)



- 
▼ Favoritos
-  Lixo Eletrônico 25
-  **Caixa de Ent... 1526**
 - Adicionar aos favor...
- 
- ▼ Pastas
-  Caixa de Entr... 1526
-  Lixo Eletrônico 25
-  Rascunhos 15
-  Itens Enviados
-  Itens Excluídos 222
-  Archive
-  Anotações 1
- Histórico de Conv...
- Nova pasta
- ▼ Grupos
- Novo grupo

← Confirming submission to Journal of South American Earth Sciences

Earth Sciences <em@editorialmanager.com>

Sex, 30/07/2021 21:16

Para: Você

This is an automated message.

Genesis of dense shell accumulation of the Middle-Eocene Man Aike Formation (Magallanes Basin, Chilean Patagonia)

Dear Mr Müller,

We have received the above referenced manuscript you submitted to Journal of South American Earth Sciences.

To track the status of your manuscript, please log in as an author at <https://www.editorialmanager.com/sames/>, and navigate to the "Submissions Being Processed" folder.

Thank you for submitting your work to this journal.

Kind regards,
Journal of South American Earth Sciences

More information and support

You will find information relevant for you as an author on Elsevier's Author Hub: <https://www.elsevier.com/authors>

FAQ: How can I reset a forgotten password? https://service.elsevier.com/app/answers/detail/a_id/28452/supporthub/publishing/

For further assistance, please visit our customer service site:

<https://service.elsevier.com/app/home/supporthub/publishing/>

Here you can search for solutions on a range of

topics, find answers to frequently asked questions, and learn more about Editorial Manager via